Line-of-Sight Spatial Modulation for Indoor mmWave Communication at 60 GHz

Peng Liu, Marco Di Renzo, Andreas Springer

Line-of-Sight (LOS) Spatial Modulation (SM) for Indoor mmWave Communication at 60 GHz

Peng Liu, *Student Member, IEEE,* Marco Di Renzo, *Senior Member, IEEE,* and Andreas Springer, *Member, IEEE*

***Abstract*—In this paper, we propose to use spatial modulation (SM) and the generalized spatial modulation (GSM) MIMO schemes in indoor line-of-sight (LOS) millimeter-wave (mmWave) communication at 60 GHz. SM/GSM are known but only at low-GHz frequencies where the channels are typically rich scattered and characterized by Rayleigh or Rician distribution. However, 60 GHz indoor channels are typically not rich but rather sparsely scattered and dominated by the LOS component, thus making them different from low-GHz fading channels and our work novel. We first seek to optimize SM in LOS by finding the channel conditions that minimize its symbol error probability (SEP). Then we extend our studies to LOS GSM and derive its channel capacity and SEP. Furthermore, we present numerical studies on the behavior and performance of SM/GSM in LOS. LOS spatial multiplexing (SMX) and beamforming (BF) MIMO schemes are used as benchmarks for comparison. At last, we propose novel TX and RX hardware architectures, both of which use only a single RF chain, for implementation of SM/GSM at mmWave frequencies. Both simplicity and good performance are exhibited by LOS SM/GSM thus making them very attractive techniques for short-range indoor mmWave communications at 60 GHz.**

***Index Terms*—Indoor millimeter-wave (mmWave) communication, line-of-sight (LOS) MIMO, 60 GHz, spatial modulation (SM), generalized spatial modulation (GSM)**

I. Introduction

MILLIMETER-wave (mmWave) communication, which is largely motivated by the global spectrum shortage at the current 2G, 3G, and 4G frequencies, is an emerging technology that provides us with multi-GHz bandwidth and enables transmission rates of multi-Gbps [1]–[3]. Especially, with up to $7\,\mathrm{GHz}$ unlicensed bandwidth available worldwide, the $60\,\mathrm{GHz}$ band ($57-64\,\mathrm{GHz}$) has gained significant interest in the industry which is evidenced e.g., by the standardization of Wireless HD, IEEE 802.15.3c, and IEEE 802.11ad [4].

A major concern with communications at mmWave frequencies is the much higher free space path loss (FSPL) due to smaller wavelength, e.g., the FSPL at $60\,\mathrm{GHz}$ is $35.6\,\mathrm{dB}$ higher than at $1\,\mathrm{GHz}$. High gains are usually needed at the transmitter (TX) and receiver (RX) to compensate for the FSPL [2]. There have been many practical works on using phased arrays and beamforming (BF) to achieve high gains for single-stream transmission [5]–[8]. However, the mmWave propagation in indoor environments is dominated by line-of-sight (LOS) components and BF achieves only array gain. On the other hand, even in LOS, enormous spatial multiplexing (SMX) gain can be achieved by using SMX-MIMO [9]–[11], thus motivating us to consider multi-stream MIMO also in indoor mmWave communications.

On one hand, multi-stream MIMO schemes based on conventional SMX are able to achieve higher data rates than single-stream transmission. On the other hand, they need N full TX chains to transmit N data streams, thus introducing significant cost and processing complexity to the system [12]. As shown by [13], SMX-MIMO, due to the use of multiple TX RF chains, is significantly inefficient in terms of the $\mathrm{bits/J}$ energy efficiency. Cost and power consumption of mmWave components are high, therefore it is unlikely to dedicate a separate RF chain and digital-to-analog converter (DAC)/analog-to-digital converter (ADC) for each antenna, but it is more likely to use fewer RF chains than the number of antennas [14], [15]. In [11], a hybrid BF/SMX architecture, which uses a smaller number of RF chains than the number of antennas, was proposed for LOS mmWave communications. In [15], a hybrid RF/baseband precoder architecture, which uses N_t^{RF} TX RF chains to transmit N data streams via N_t TX antennas (where $N \leq N_t^{\mathrm{RF}} \leq N_t$), was proposed for sparsely scattered mmWave channels. However, in both examples, N (or more) RF chains are still needed for transmission of N data streams.

We propose to use the simpler and more energy-efficient spatial modulation (SM) and its generalization the generalized spatial modulation (GSM) [12], [16]–[18] in indoor mmWave communications. As depicted in Fig. 1, SM/GSM is capable of transmitting two streams — one in the spatial domain and the other in the conventional in-phase and quadrature (IQ) domain — using a single TX RF chain. The benefits of using SM/GSM are comprehensively addressed in [18]. Here we highlight: 1) reduced complexity and cost due to the fact that SM/GSM needs only one TX RF chain; 2) significantly improved energy efficiency at the TX [13]; and 3) the single RF plus antenna switching architecture seems to be a very attractive solution for large scale MIMO.

At mmWave frequencies, the indoor propagation is quasi-optical, sparsely scattered and with large reflection and blockage losses (see Section II-C). Therefore, in this

P. Liu and A. Springer are with the Institute for Communications Engineering and RF-Systems (NTHFS), Johannes Kepler University (JKU), Linz, Austria. (e-mail: {p.liu,a.springer}@nthfs.jku.at). Their work is in part supported by the Austrian COMET-K2 programme of the Linz Center of Mechatronics (LCM), which is funded by the Austrian federal government and the federal state of Upper Austria.

M. Di Renzo is with the Laboratoire des Signaux et Systèmes, CNRS, CentraleSupélec, Univ Paris Sud, Université Paris-Saclay, 3 rue Joliot Curie, Plateau du Moulon, 91192, Gif-sur-Yvette, France. (e-mail: marco.direnzo@l2s.centralesupelec.fr). His work is partially supported by the European Commission (EC) through the H2020-ETN-5Gwireless research project (grant 641985) and by the Agence Nationale de la Recherche Scientifique (ANR) through the SpatialModulation research project (Société de l'Information et de la Communication – Action Plan 2015).

paper, we only consider the dominant LOS components. In a rich-scattering environment at low-GHz frequencies, antennas with separations down to $\lambda/2$ can lead to sufficiently small channel correlations and a high rank[1] MIMO channel can easily be established to support simultaneous transmission of multiple data streams [19]. However, in a strong LOS environment, the principle of so-called LOS-MIMO [9]–[11], [20] should be utilized to achieve high capacity. LOS-MIMO relies on appropriate separation of the antennas, which is in general much larger than $\lambda/2$, to achieve a high rank channel and thus high capacity [9]. The optimal antenna separation depends on both the wavelength and the TX-RX distance (see Section III-C). A shorter wavelength and smaller TX-RX distance both lead to a smaller optimal antenna separation, thus making LOS-MIMO more practical for short-range indoor mmWave communications.

We first study the symbol error probability (SEP) and channel capacity of LOS SM/GSM based on a (full-complexity) maximum likelihood (ML) RX. Then we propose and study practical TX and (reduced-complexity) RX architectures. The SEP of the ML RX is used as a benchmark in the SEP study of the proposed RX. The novelty and major contributions of this paper are summarized as follows:

- We propose to use SM/GSM for indoor LOS mmWave communication at $60\,\mathrm{GHz}$, which is not yet seen in the mmWave literature. Although SM/GSM are known schemes, they have only been considered and applied at low-GHz frequencies, where the channel characteristics are typically Rayleigh or Rician fading. Due to the randomness and low correlation of rich scattered fading channels, SM/GSM in low-GHz fading channels generally does not need excess antenna separations and down to $\lambda/2$ antenna separations were used in practice [21]–[23]. However, the $60\,\mathrm{GHz}$ indoor channel is not rich but rather sparsely scattered and dominated by LOS components and thus is different from typical low-GHz channels [24].
- We try to minimize the SEP of SM in LOS by maximizing the minimum Euclidean distance of the RX-side SM symbols $\Phi_{\min}$. As a result, we find that the (column) channel orthogonality condition (21) is a condition that maximizes $\Phi_{\min}$ and thus optimizes the SEP. Since it requires proper (inter-element) separation of the TX and RX antennas in order to achieve (21), it turns out that optimized SEP of LOS SM requires proper separation of TX and RX antennas.
- We derive the channel capacity and SEP for LOS GSM, which is a natural generalization of LOS SM for higher data rates while still using a single TX RF chain and the same number of antennas. The analyses and results based on LOS channels are novel. Our numerical results and further analysis in Section V bring further insight into the behavior and performance of SM/GSM in LOS. In addition, we study the robustness of condition (21) and the impact of not having perfect orthogonality.

[1]The rank of a channel matrix is equal to the number of linearly independent rows or columns of the channel matrix [9].

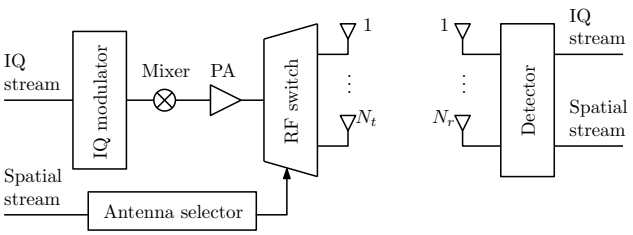

Fig. 1. Conceptual block diagram for SM/GSM.

- We propose novel TX and RX hardware architectures, both of which use only a single RF chain, for implementation of SM/GSM at mmWave frequencies. The proposed TX features a parallel shunt switching structure and a flexible power delivering network. The number of power amplifiers (PAs) (at design phase) can be selected according to the link power budget. The proposed RX features hybrid RF/digital processing and separate detection of the spatial and IQ streams.

To the best of our knowledge, the only closely related works are [25] and [26]. In [25], a so-called antenna subset modulation (ASM) scheme, which is also based on the antenna switching principle, was introduced to mmWave communication. However, in ASM the purpose of antenna switching was for communication security but not directly used for carrying information bits. In [26], LOS space shift keying (SSK) was proposed for indoor mmWave communication and the same orthogonality condition (21) was used. However, since SSK does not transmit an IQ stream, there was no consideration of an IQ constellation and the optimality of the orthogonality condition for LOS SM/GSM was not clear.

The rest of the paper is organized as follows. In Section II, we describe the principle of SM/GSM and the system and channel models. In Section III, we optimize LOS SM by finding the channel conditions that minimize its SEP. In Section IV, we derive the channel capacity and SEP generally for LOS GSM. In Section V, we present numerical results for LOS SM/GSM and compare with LOS SMX and BF. Furthermore we perform an analysis of the robustness of the orthogonality condition and the impact of not having perfect orthogonality. In Section VI, we propose novel TX and RX hardware architectures for implementation of SM/GSM at mmWave frequencies. Finally, Section VII concludes the paper.

II. Principle and System Model

A. Principle of SM/GSM

As depicted in Fig. 1, SM/GSM can transmit two data streams, namely an IQ stream and a spatial stream, using a single TX RF chain. The bits of the IQ stream are modulated using a conventional IQ modulation scheme, e.g., quadrature amplitude modulation (QAM) or phase shift keying (PSK), and the bits of the spatial stream are mapped into TX antenna indices, based on which one or more TX antennas are activated. In SM, only a single TX antenna is activated per channel use. However, in GSM, N_u TX antennas can be activated per channel use, where N_u can be varied for different symbols. For simplicity, we restrict our studies to SM and fixed-N_u

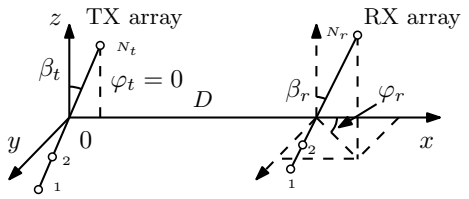

Fig. 2. LOS MIMO using arbitrarily placed ULAs. The coordinate system is chosen such that the center of the TX ULA locates at the origin and the center of the RX ULA lies on the x-axis. Furthermore, the TX ULA lies in the xz-plane, i.e., $\varphi_t = 0$.

GSM (a.k.a. GSM-N_u). Apparently, SM is a special case of GSM-N_u with $N_u = 1$. SM achieves a rate of $\log_2 N_t$ in the spatial domain and a total rate of $\log_2 N_t + \log_2 M$, where M is the IQ constellation size. GSM-N_u achieves a spatial rate of $\log_2 \binom{N_t}{N_u}$ and a total rate of $\log_2 \binom{N_t}{N_u} + \log_2 M$ [16]. Apparently, higher data rates can be achieved by GSM with the same number of TX antennas. Note that we do not restrict the number of antenna combinations to an integer power of two. Therefore, the spatial rate $\log_2 \binom{N_t}{N_u}$ can be a fractional number[2].

B. Antenna Array

As shown in Fig. 2, we consider an $N_t \times N_r$ LOS MIMO system using two arbitrarily placed uniform linear arrays (ULAs), where N_t is the number of TX antennas and N_r is the number of RX antennas. The antenna separations in the TX and RX ULAs are respectively s_t and s_r, and the TX-RX distance is D, which is measured between the center points of the TX and RX ULAs. Geometrically, the ULAs each have two degrees of freedom, namely the azimuth angle φ and the tilt angle β (or equivalently the elevation angle $\theta = \pi/2 - \beta$). Since we are only interested in their relative geometric relations, only three angles are used — the tilt angles β_t and β_r respectively at the TX and RX and the azimuth angle φ_r at the RX. Note that we limit β_t and β_r to $[0, \pi/2]$ yet are still being able to cover all cases.

We do not consider the physical implementation and radiation pattern of the antennas, but assume that the antennas have the same gain at the LOS directions.

C. 60 GHz Indoor Channel Model

As stated in Section I, in this paper we consider only a pure LOS channel. In this section, before we describe the pure LOS channel model, we first elaborate on why we only consider LOS components and in which scenarios the pure LOS channel model fits.

Indoor propagation at 60 GHz shows the following characteristics:

1) The propagation at mmWave frequencies exhibits a quasi-optical behavior with most of the signal energy being received along the LOS path and a few reflected paths. Measured results show that geometry-optical ray-tracing covers the transmission characteristics well and the transmission path loss is well predicted by the Friis transmission equation [29]–[31].
2) High reflection loss. It was shown in [30] by measurements that each reflection at the walls or ceiling typically introduces a reflection loss of 10 dB. It is thus common to consider only up to second order reflections, which have 20 dB reflection loss on average and additional path loss due to increased path lengths as compared to the LOS path.
3) Blockage and penetration losses are generally higher at higher frequencies. The blockage loss of a human body is typically 20 dB and the blockage loss of a 1-cm-thick wooden barrier is about 10 dB [6]. The practical indoor operation range at 60 GHz is likely to be limited by penetration loss and therefore mostly confined to a single room [32].

According to the above description of the propagation characteristics and further details of the IEEE802.11ad (60 GHz WLAN) indoor channel model [24], it is evident that the 60 GHz indoor channel is dominated by LOS components. The non-line-of-sight (NLOS) components, depending on the beamwidth and position of the antennas, include only few highly attenuated rays[3]. These facts motivate us to design our scheme only based on LOS components, while ignoring the NLOS components.

The LOS MIMO channel can be described using an $N_r \times N_t$ matrix as

$$\mathbf{H} = \begin{bmatrix} h_{11} & \cdots & h_{1N_t} \\ \vdots & \ddots & \vdots \\ h_{N_r1} & \cdots & h_{N_rN_t} \end{bmatrix}, \tag{1}$$

where h_{ji} is the LOS component of the channel impulse response from the i-th TX antenna to the j-th RX antenna, and is normalized by the FSPL due to the TX-RX distance D. According to the Friis equation [29], h_{ji} is calculated as

$$h_{ji} = \frac{\lambda}{4\pi d_{ji}} \exp(-\mathbb{j}kd_{ji}) \cdot \frac{4\pi D}{\lambda} \approx \exp(-\mathbb{j}kd_{ji}) \tag{2}$$

where $k = 2\pi/\lambda$ is the wave number, d_{ji} is length of the LOS path between the i-th TX antenna and the j-th RX antenna, $\mathbb{j}$ is the complex unit. For the approximation in (2) to hold, we have assumed that the TX and RX array lengths L_t, L_r are much smaller than D, i.e., $L_t, L_r \ll D$.

III. Error Performance Optimization of LOS SM

In this section, we seek to find the channel conditions that optimize the error performance of SM in LOS. We first give the SEP expression for LOS SM using an ML detector. Then

[2]Fractional bits transmission can be achieved e.g., using the fractional bit modulation given in [27] which is based on the modulus conversion theory, or the bit-padding method given in [28] which maps different bit lengths onto the indices of the TX antennas.

[3]For example, in the STA-STA (device-to-device) sub-scenario [24, Section 3.3], if the azimuth beam angles of the TX and RX antennas do not exceed $\pm 62°$, all the first order clusters from walls will be eliminated, because none of them have TX and RX azimuth angles simultaneously falling in this azimuth beam range [24, Figure 9]. If the elevation beam angles of the TX and RX antennas are less than $56.6°$, the (only) first order cluster reflected by ceiling is eliminated as well [24, Figure 10]. Meanwhile, most of the second order clusters [24, Figure 11], which are weaker than the first order clusters due to one more reflection and longer path lengths, are eliminated as well.

we formulate the optimization problem in a tractable manner, i.e., in terms of maximizing the minimum Euclidean distance of the RX symbols. Upon solving the optimization problem, we will find the channel conditions that can optimize the error performance of SM in LOS. At the end, we compare the optimal channel conditions found for LOS SM with the optimal conditions for LOS SMX.

A. Spatial Modulation and ML Detection

The SM modulation alphabet is defined as

$$\mathbb{S} = \left\{ q_m \cdot \underbrace{[\cdots, 0, \overbrace{1}^{i\text{-th}}, 0, \cdots]^{\mathsf{T}}}_{\mathbf{e}_i} \;\middle|\; \begin{array}{c} i = 1, \cdots, N_t \\ m = 1, \cdots, M \end{array} \right\}, \quad (3)$$

where q_m is an IQ symbol, and M is the IQ constellation size. The definition of $\mathbb{S}$ reflects the fact that in SM the information is modulated not only in the traditional IQ domain but also in the spatial domain (by selecting one out of N_t TX antennas for activation). The received signal vector $\mathbf{y} \in \mathbb{C}^{N_r \times 1}$ is given by

$$\mathbf{y} = \mathbf{H}\mathbf{s}_{i,m} + \mathbf{n} = q_m \mathbf{h}_i + \mathbf{n} \quad (4)$$

where $\mathbf{s}_{i,m} \in \mathbb{S}$ is the transmitted SM symbol, $\mathbf{h}_i$ is the i-th column of $\mathbf{H}$, $\mathbf{n} \in \mathbb{C}^{N_r \times 1}$ is an independent and identically distributed (i.i.d.) complex additive white Gaussian noise (AWGN) vector with covariance matrix $N_0\mathbf{I}_{N_r}$ (where $\mathbf{I}_{N_r}$ is an $N_r \times N_r$ identity matrix). Due to single antenna activation at the TX, the received signal vector at the RX contains only a single column of the channel matrix multiplied by an IQ symbol. This is different from SMX-MIMO, in which the received signal typically contains a combination of all columns of the channel matrix.

The optimal (ML) detection of the SM symbols requires joint detection of i and m [33], i.e.,

$$(\hat{\imath}, \hat{m}) = \arg\max_{i,m} p_{\mathbf{y}}\left(\mathbf{y} \,|\mathbf{s}_{i,m}, \mathbf{H}\right) \quad (5a)$$

$$= \arg\min_{i,m} \|\mathbf{y} - q_m \mathbf{h}_i\|, \quad (5b)$$

where $p_{\mathbf{y}}(\cdot)$ is the probability density function (PDF) of $\mathbf{y}$, and $\|\cdot\|$ evaluates the Euclidean distance.

B. SEP of LOS SM and Optimization

A tight upper bound for the SEP of LOS SM, which is based on the union bound method and derived for the ML detector (5) [34], is given by

$$P_s \leq \frac{1}{MN_t} \sum_{i,m} \sum_{\substack{i',m' \\ (i',m') \neq (i,m)}} \Pr[(i,m) \to (i',m')|(i,m)], \quad (6)$$

where $\Pr[(i,m) \to (i',m')|(i,m)]$ is a pairwise error probability that denotes the probability of (i',m') being detected given that (i,m) was sent. $\Pr[(i,m) \to (i',m')|(i,m)]$ can be calculated as

$$\begin{aligned}
&\Pr[(i,m) \to (i',m')|(i,m)] \\
&= \Pr\left[\, \|\mathbf{y} - q_{m'}\mathbf{h}_{i'}\| < \|\mathbf{y} - q_m \mathbf{h}_i\| \,\right] \\
&= \Pr\left[\, \|q_m\mathbf{h}_i - q_{m'}\mathbf{h}_{i'} + \mathbf{n}\|^2 < \|\mathbf{n}\|^2 \,\right] \\
&= \Pr\left[\, (q_m\mathbf{h}_i - q_{m'}\mathbf{h}_{i'} + \mathbf{n})^{\mathrm{H}} (q_m\mathbf{h}_i - q_{m'}\mathbf{h}_{i'} + \mathbf{n}) < \mathbf{n}^{\mathrm{H}}\mathbf{n} \right] \\
&= \Pr\left[\, \|q_m\mathbf{h}_i - q_{m'}\mathbf{h}_{i'}\|^2 < \underbrace{2\Re\left\{(q_{m'}\mathbf{h}_{i'} - q_m\mathbf{h}_i)^{\mathrm{H}}\,\mathbf{n}\right\}}_{n_\Sigma} \,\right] \\
&= Q\left(\sqrt{\frac{\Phi}{2N_0}}\right), \quad (7)
\end{aligned}$$

where n_Σ, which is a simplified notation for $n_\Sigma(i,m,i',m')$, is Gaussian distributed

$$n_\Sigma \sim \mathcal{N}\left(0, 2\|q_{m'}\mathbf{h}_{i'} - q_m\mathbf{h}_i\|^2 N_0\right),$$

and Φ, which is a simplified notation for $\Phi(i,m,i',m')$, is the squared Euclidean distance between two RX-side SM symbols

$$\Phi = \|q_m\mathbf{h}_i - q_{m'}\mathbf{h}_{i'}\|^2, \quad (8)$$

and $Q(\cdot)$ is the Gaussian Q-function. Although sharing the same union bound method, (6) is different from the average error probability given in [34, (9)] for SM in fading channels. In fading channels, the error probability must be averaged over the fading channel statistics [34]. However, in our case, the channel is deterministic and (6) including its optimization below are unique to (pure) LOS channels. Furthermore, for conventional SM in a rich scattered environment, the channel is random and only the IQ constellation $\{q_m\}$ can be taken as a parameter for optimization but not the channel. In this paper, since the channel is deterministic and determined by the geometric relations between the antennas, we can optimize the performance of LOS SM by optimizing the channel via choosing suitable antenna separations. This is a novelty of our work, and in Section III-D we will further address this.

Equation (6) indicates that the SEP depends on all possible pairs of the SM symbol Euclidean distances. To minimize the error probability, in general we wish to maximize all the SM symbol Euclidean distances simultaneously. However, we maximize the minimum symbol Euclidean distance since at high signal-to-noise ratio (SNR) P_s is limited by the smallest symbol Euclidean distance [35, ch. 4]. This optimization problem can be formulated as

$$\underset{\{q_m\},\{\mathbf{h}_i\}}{\text{maximize}} \quad \underbrace{\min_{i,i',m,m',(i,m)\neq(i',m')} \|q_m\mathbf{h}_i - q_{m'}\mathbf{h}_{i'}\|^2}_{\triangleq \Phi_{\min}}. \quad (9)$$

There is also an implicit constraint that $\{\mathbf{h}_i\}$, which is determined by N_t, N_r, s_t, s_r, φ_t, β_t, β_r and D, needs to be realizable using ULAs. To make the optimization problem (9) tractable, we break down the pairwise Euclidean distance Φ of SM symbols into three cases, and assume that the IQ constellation $\{q_m\}$ is independent of $\{\mathbf{h}_i\}$, i.e., we only consider optimizing $\{\mathbf{h}_i\}$. For ease of presentation, we assume that the IQ constellation is either M-PSK or M-QAM (with

square, rectangular, or circular constellations [35, ch. 3–4]), which are the most commonly used constellations.

1) Case I ($i = i'$ and $m \neq m'$, i.e. correct spatial symbol and wrong IQ symbol): Because of (2), we have $\|\mathbf{h}_i\| = \sqrt{N_r}$, thus $\Phi_{\min}$ in this case can be found from (8) to be

$$\Phi_{\min}^{(1)} = \min_{i,m,m'} \|\mathbf{h}_i\|^2 |q_m - q_{m'}|^2 = N_r d_{\min}^2, \tag{10}$$

where $d_{\min} = \min_{m,m'(m\neq m')} |q_m - q_{m'}|$ is the minimum symbol distance in the IQ constellation.

2) Case II ($i \neq i'$ and $m = m'$, i.e. wrong spatial symbol and correct IQ symbol): In this case (8) can be written into

$$\Phi = \|\mathbf{h}_i - \mathbf{h}_{i'}\|^2 r_m^2 = 2N_r \left(1 - \cos\theta(i,i')\right) r_m^2 \tag{11}$$

where $r_m = |q_m|$ is the magnitude of q_m, and $\theta(i,i')$ is the Euclidean angle [36] between $\mathbf{h}_i$ and $\mathbf{h}_{i'}$ defined as

$$\theta(i,i') = \arccos \frac{\Re\{\langle \mathbf{h}_i, \mathbf{h}_{i'} \rangle\}}{\|\mathbf{h}_i\| \|\mathbf{h}_{i'}\|} \in [0, \pi], \tag{12}$$

where $\langle \cdot, \cdot \rangle$ is the Hermitian inner product defined as $\langle \mathbf{v}, \mathbf{w} \rangle = \mathbf{v}^\intercal \mathbf{w}^*$, and $(\cdot)^\intercal$ and $(\cdot)^*$ are respectively the transpose and conjugate operators. Since $1 - \cos\theta$ is an increasing function over $[0, \pi]$, $\Phi_{\min}$ in this case is found from (11) to be

$$\Phi_{\min}^{(2)} = 2N_r r_{\min}^2 \left(1 - \cos\theta_{\min}\right), \tag{13}$$

where $r_{\min} = \min_m r_m$, and $\theta_{\min} = \min_{i,i'(i\neq i')} \theta(i,i')$.

3) Case III ($i \neq i'$ and $m \neq m'$, i.e. wrong spatial symbol and wrong IQ symbol): According to Appendix A, we have

$$\Phi \geq N_r \left[r_m^2 + r_{m'}^2 - 2r_m r_{m'} \cos\theta_{\mathrm{H}}(i,i')\right] \tag{14a}$$

$$= N_r \left[(r_m - r_{m'})^2 + 2r_m r_{m'} \left(1 - \cos\theta_{\mathrm{H}}(i,i')\right)\right] \tag{14b}$$

$$\geq 2N_r r_m r_{m'} \left(1 - \cos\theta_{\mathrm{H}}(i,i')\right), \tag{14c}$$

where $\theta_{\mathrm{H}}(i,i') \in [0, \pi/2]$ is the so-called Hermitian angle (see Appendix A). Since $1 - \cos\theta_{\mathrm{H}}$ is an increasing function over $[0, \pi/2]$, $\Phi_{\min}$ in this case is found from (14c) to be

$$\Phi_{\min}^{(3)} = 2N_r r_{\min}^2 \left(1 - \cos\theta_{\mathrm{H,min}}\right), \tag{15}$$

where $\theta_{\mathrm{H,min}} = \min_{i,i'(i\neq i')} \theta_{\mathrm{H}}(i,i')$.

The global $\Phi_{\min}$ is therefore given by

$$\Phi_{\min} = \min\left\{\Phi_{\min}^{(1)}, \Phi_{\min}^{(2)}, \Phi_{\min}^{(3)}\right\} = N_r \min\left\{d_{\min}^2, 2r_{\min}^2 \left(1 - \cos\theta_{\min}\right), 2r_{\min}^2 \left(1 - \cos\theta_{\mathrm{H,min}}\right)\right\}. \tag{16}$$

The system shows an RX array gain of N_r. However, more important than increasing N_r is to "choose" $\theta_{\min}$ and $\theta_{\mathrm{H,min}}$ properly, otherwise $\Phi_{\min}$ in (16) can still be very small or even zero regardless of N_r. In what follows, we take $\theta_{\min}$ and $\theta_{\mathrm{H,min}}$ as variables to maximize $\Phi_{\min}$. Consider the following facts: 1) $0 \leq \Phi_{\min}^{(2)} \leq 4N_r r_{\min}^2$, because $\theta(i,i') \in [0, \pi]$; 2) $0 \leq \Phi_{\min}^{(3)} \leq 2N_r r_{\min}^2$, because $\theta_{\mathrm{H}}(i,i') \in [0, \pi/2]$; 3) for QAM, $d_{\min}^2 = 2r_{\min}^2$ [35]; 4) for $M(M \geq 4)$-PSK, $d_{\min}^2 = 4r_{\min}^2 \sin^2\left(\pi/M\right) \leq 2r_{\min}^2$; 5) for BPSK, $d_{\min}^2 = 4r_{\min}^2$. It is clear that the maximum possible $\Phi_{\min}$, which we denote as $\widehat{\Phi}_{\min}$, for QAM and $M(M \geq 4)$-PSK is given by

$$\widehat{\Phi}_{\min} = \Phi_{\min}^{(1)} = N_r d_{\min}^2, \tag{17}$$

and for BPSK by

$$\widehat{\Phi}_{\min} = \max_{\theta_{\mathrm{H,min}}} \Phi_{\min}^{(3)} = 2N_r r_{\min}^2. \tag{18}$$

To achieve (17), we need

$$\begin{cases} 2r_{\min}^2 \left(1 - \cos\theta_{\min}\right) \geq d_{\min}^2, & \text{(19a)} \\ 2r_{\min}^2 \left(1 - \cos\theta_{\mathrm{H,min}}\right) \geq d_{\min}^2, & \text{(19b)} \end{cases}$$

which in turn requires

$$\begin{cases} \theta_0 \leq \theta_{\min} \leq \pi, & \text{(20a)} \\ \theta_0 \leq \theta_{\mathrm{H,min}} \leq \pi/2, & \text{(20b)} \end{cases}$$

where $\theta_0 \triangleq \arccos(1 - d_{\min}^2/(2r_{\min}^2))$ with $\arccos(\cdot)$ being restricted to $[0, \pi]$.

Since for QAM we have $d_{\min}^2 = 2r_{\min}^2$ and $\theta_0 = \pi/2$, (20b) reduces to $\theta_{\mathrm{H,min}} = \pi/2$, or equivalently $\theta_{\mathrm{H}}(i,i') = \pi/2, \ \forall i, i'(i \neq i')$, which, because of (49) and (50) in Appendix A, is equivalent to

$$\langle \mathbf{h}_i, \mathbf{h}_{i'} \rangle_{i\neq i'} = 0 \quad \forall i, i' \in \{1, 2, \cdots, N_t\}. \tag{21}$$

Equation (21) in turn leads to $\theta(i,i') = \pi/2 \, \forall i, i'(i \neq i')$ and satisfies (20a). Apparently (21) also satisfies (20) and (19) and achieves (17). To achieve (18), it can be shown that we also need (21).

In summary, we have found (21) as a solution to maximize $\Phi_{\min}$ for LOS SM using M-QAM or M-PSK in the IQ domain. The above analysis is validated by numerical simulations which are based on an exhaustive search of $\Phi_{\min}$ (over $\{\Phi_{i,m,i',m'} | (i,m) \neq (i',m')\}$). The simulation results are omitted here due to the page limit.

Under condition (21), the SEP in (6) can be further simplified. However, we delay this to Section IV-C, where we will derive the SEP for LOS GSM using (21).

C. Orthogonal Channel Construction

To achieve (21), the antenna separation product (ASP) $s_t s_r$ has to be chosen properly, and the optimal ASP that leads to (21) has previously been derived in [9], [10], [19]. Using the coordinates of Fig. 2 and following the derivation of [9], we have

$$d_{ji} - d_{ji'} \approx (j-1)P + R, \tag{22}$$

where $P = 1/D \cdot (i' - i) s_t s_r \cos\beta_t \cos\beta_r$, $R = (i' - i) s_t \sin\beta_t + 1/(2D) \cdot [-(i + i' - 2) s_t \cos\beta_t + L_t \cos\beta_t - L_r \cos\beta_r](i' - i) s_t \cos\beta_t$. Thus

$$\begin{aligned} \langle \mathbf{h}_i, \mathbf{h}_{i'} \rangle_{i\neq i'} &= \sum_{j=1}^{N_r} \exp\left[-\mathbb{j} k (d_{ji} - d_{ji'})\right] \\ &\approx \sum_{j=1}^{N_r} \exp\left[-\mathbb{j} k \left[(j-1)P + R\right]\right] \\ &= \frac{1 - \exp\left(-\mathbb{j} k N_r P\right)}{1 - \exp\left(-\mathbb{j} k P\right)} \exp\left(-\mathbb{j} k R\right) \\ &= \underbrace{\sin\left(\frac{k N_r P}{2}\right) \Big/ \sin\left(\frac{kP}{2}\right)}_{I} \times J, \end{aligned} \tag{23}$$

where $J = \exp[-\jmath k((N_r-1)P/2+R)]$. Since there is no general solution for $J=0$, we have to force $I=0$ in order to achieve (21). Note that (23) generates a group of $\binom{N_t}{2}$ conditions for all $i,i' \in \{1,\cdots,N_t\}$ and $i \neq i'$. These conditions together lead to the optimum ASP

$$s_t s_r \approx nD\lambda\zeta/N_r, \tag{24}$$

where $\zeta \triangleq 1/(\cos\beta_t \cos\beta_r)$, $n \in \mathbb{Z}^+ \backslash \{pN_r/q | p \in \mathbb{Z}^+, q = 1,...,N_t-1\}$, and $N_r \geq N_t \geq 2$. In (24), ζ is termed tilt factor which measures the degree of tilt of the ULAs. Since $\beta_t, \beta_r \in [0, \pi/2]$, it holds that $\zeta \geq 1$. When the ULAs are parallel and aligned, i.e., $\beta_t = \beta_r = 0$, we have $\zeta = 1$, i.e., no tilt. For minimum antenna separations we choose $n=1$ and the condition becomes

$$s_t s_r \approx D\lambda\zeta/N_r, \quad \text{and } N_r \geq N_t \geq 2. \tag{25}$$

Perfect orthogonality will be lost if the actual ASP differs from the optimal value. To measure this, we use an ASP deviation factor η which was previously defined in [9] as

$$\eta = \frac{\text{Minimum ASP for orthogonality}}{\text{Actual ASP}} = \frac{D\lambda\zeta/N_r}{s_t s_r}, \tag{26}$$

where the minimum ASP for orthogonality is given in (25). Further note that the $s_t s_r$ in the demoninator of (26) denotes the actual ASP and should not be confused with the optimal ASP (to achieve channel orthogonality) given in (25). If the actual ASP is larger than the optimal ASP, we have $\eta < 1$; if the actual ASP is smaller than the optimal ASP, we have $\eta > 1$. In what follows, we use η as an (inverted) normalized ASP.

D. Comparison with LOS SMX-MIMO

Although (21) is the same as the column orthogonality condition used in LOS SMX-MIMO for the case of $N_r \geq N_t$ [9], [11], it is important to notice that the underlying problems are different. We address the main differences as follows:

1) The optimization problems are different. In the LOS SMX-MIMO literature, e.g., [9]–[11], the goal was to find the optimal antenna separations that maximize the SMX channel capacity, and (21) was found as a solution for the case of $N_r \geq N_t$. The essence is that (21) guarantees $\mathbf{H}$ having N_t equal eigenvalues, thus the SMX capacity is maximized [9]. However, in our case, due to the unavailability of a closed-form expression for the SM channel capacity (see Section IV-B), we instead seek to optimize the SEP of SM. The essence here is that (21) minimizes the SEP of SM by maximizing the minimum Euclidean distance of the RX-side SM symbols.
2) The requirements on the array dimensions are not exactly the same. In our case, we need $N_r \geq N_t$ in order to achieve the column orthogonality (21). However, in LOS SMX-MIMO, there are two cases: if $N_r \geq N_t$, the column orthogonal condition (21) is optimal; if $N_t \geq N_r$, the optimal solution is a row orthogonal condition [10]. As a result, in any case, $\min(N_t, N_r)$ number of data streams can be transmitted.

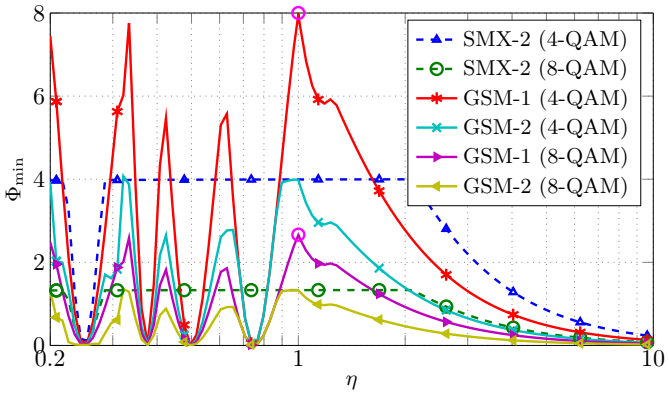

Fig. 3. The minimum Euclidean distance of the RX-side symbols $\Phi_{\min}$ vs. ASP for different LOS MIMO schemes. We assume: 4×4 ($N_t \times N_r$) MIMO with parallel and aligned ULAs (i.e., $\zeta = 1$), $f = 60\,\text{GHz}$, $s_t = s_r$ and $D = 3\,\text{m}$. SMX-2 denotes SMX with two parallel IQ streams. Different IQ constellations are used and indicated in the legend. The curves are generated numerically based on exhaustive searches for $\Phi_{\min}$. The two magenta circles, which fall on the respective curves for GSM-1 (4-QAM) and GSM-1 (8-QAM), are calculated from (17). The derivations for (17) are apparently validated.

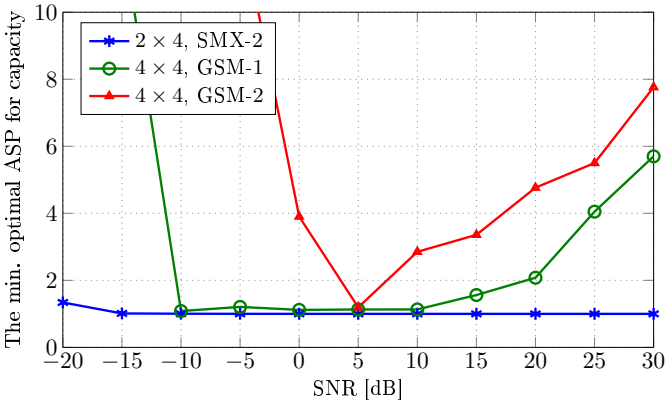

Fig. 4. The minimum optimal ASP needed to maximize the channel capacity of different LOS systems. The optimal ASPs are found by numerical optimization of (30) for SM/GSM and the first step of (46) for SMX. For all systems we assume parallel and aligned ULAs (i.e., $\zeta = 1$), $f = 60\,\text{GHz}$, $s_t = s_r$ and $D = 3\,\text{m}$. In the legend, the MIMO size is indicated in the format $N_t \times N_r$, and SMX-2 denotes SMX with two parallel IQ streams. The SNR is defined as the ratio of the TX power to the RX noise power.

3) The meaning of (21) is different for the two kinds of systems. To maximize $\Phi_{\min}$ (thus to minimize SEP), it is confirmed by numerical results (see Fig. 3 for the cases with 4-QAM and 8-QAM) that (21) is in general a necessary and sufficient condition for LOS SM/GSM using QAM and $M(M \leq 8)$-PSK constellations; however, (21), though sufficient, is not a necessary condition to maximize $\Phi_{\min}$ for LOS SMX. If we seek to optimize the capacity, the simulation results in Fig. 4 indicate that (21), which corresponds to $\eta = 1$, is necessary to optimize the capacity of LOS SMX. This result was already proved in [11] and therefore is expected. However, to maximize the capacity of LOS SM/GSM, (21) tends to be needed only at moderate SNR.

IV. Capacity and SEP of LOS GSM

As introduced in Section II-A, GSM is a generalization of SM which can achieve higher data rates in the spatial domain by activating more than one TX antenna per channel use. In this section, we consider fixed-N_u GSM (a.k.a GSM-N_u) and derive its capacity and SEP based on the framework of LOS SM. The meaningfulness of LOS GSM is enhanced by the fact that (21) also maximizes $\Phi_{\min}$ for LOS GSM (see also item 3 in Section III-D). In the capacity derivation, we assume no channel state information at TX (CSIT) but perfect channel state information at RX (CSIR). In the SEP derivation, as already implicitly done in the previous section, we assume that $\mathbf{H}$ is known at the RX.

A. Extended Channel Model

The SM system model (4) can be extended for GSM-N_u as

$$\mathbf{y} = \mathbf{H} \cdot \frac{\mathbf{e}_i}{\sqrt{N_u}} \cdot s + \mathbf{n} = \frac{s}{\sqrt{N_u}} \sum_{k \in \mathcal{I}_i} \mathbf{h}_k + \mathbf{n}, \tag{27}$$

where $\mathbf{e}_i$ is an $N_t \times 1$ vector composed of N_u 1's and $N_t - N_u$ 0's, and $\mathcal{I}_i = \{k | \, k \in \{1, \cdots, N_t\} \text{ and } \mathbf{e}_i(k) = 1\}$ is the set of indices of the activated TX antennas corresponding to $\mathbf{e}_i$. According to these definitions we have $\left|\{\mathbf{e}_i\}\right| = \binom{N_t}{N_u}$ (where $|\cdot|$ for a set denotes its cardinality) and $|\mathcal{I}_i| = N_u$.

Specifically, when the orthogonality condition (21) is fulfilled, we can write (27) into an equivalent system model[4]

$$\tilde{\mathbf{y}} = \sqrt{N_r}\mathbf{H}^{\dagger}\mathbf{y} = \sqrt{\frac{N_r}{N_u}}\mathbf{e}_i s + \tilde{\mathbf{n}} \tag{28}$$

where $\tilde{\mathbf{n}} \sim C\mathcal{N}(\mathbf{0}, N_0\mathbf{I}_{N_t})$.

B. Capacity

The mutual information between the input and output of the system model (27) can be calculated, according to the chain rule for information as [37]

$$I(i, s; \mathbf{y}) = I(s; \mathbf{y}|i) + I(i; \mathbf{y}). \tag{29}$$

Equation (29) indicates that the mutual information of the GSM channel is the sum of the average mutual information (over i) of the (conventional) IQ channels and the mutual information of the spatial channel. Therefore the (total) channel capacity can be written as $C = C_1 + C_2$, where C_1 and C_2 are respectively the IQ domain mutual information and spatial domain mutual information that correspond to the two terms on the right-hand side of (29). The optimal signaling of i and s, and the (total) channel capacity C can be found by maximizing $I(i, s; \mathbf{y})$ with respect to $p(i)$ (the probability mass function (PMF) of i) and $p(s)$ (the PDF of s). However, because the channel input contains both discrete and continuous signals, finding a solution for the optimal signaling of i and s is not easily possible. Below we use a simple signaling scheme — zero-mean complex Gaussian (ZMCG) signaling in the IQ domain and uniform signaling in the spatial domain — that was first used in [37]. ZMCG signaling is known to be optimal in the IQ domain, and equal use of the antenna groups is also reasonable when CSIT is not available due to two reasons: 1) without CSIT we have no information about which antenna group should be more often used; 2) uniform distribution of i maximizes the information modulated on the spatial dimension. On the other hand, the signaling scheme is strictly not optimal and we will address the sub-optimality issue at the end of this subsection.

Theorem 1. *The capacity achieved by LOS GSM-N_u with ZMCG signaling in the IQ domain and uniform signaling in the spatial domain is given by*

$$\begin{aligned} C = & \underbrace{\sum_i p(i) \left[\log_2 \left(1 + \frac{E_s}{N_u N_0} \left\| \sum_{k \in \mathcal{I}_i} \mathbf{h}_k \right\|^2 \right) \right]}_{C_1} \\ & + \underbrace{\log_2 \tbinom{N_t}{N_u} - \frac{1}{\binom{N_t}{N_u}} \sum_i \mathbb{E}_{\mathbf{y}|i} \left[\log_2 \frac{\sum_{i'} p(\mathbf{y}|i')}{p(\mathbf{y}|i)} \right]}_{C_2}, \end{aligned} \tag{30}$$

where E_s is the average energy of the IQ symbol, $\mathbb{E}_{\mathbf{y}|i}[\cdot]$ is the expectation over conditional random vector $\mathbf{y}$ (conditioned on i), $p(i)$ is the PMF of i, $p(\mathbf{y}|i)$ is the conditional PDF of $\mathbf{y}$ given by

$$p(\mathbf{y}|i) = \frac{1}{|\pi \mathbf{\Gamma}_i|} \exp\left[-\mathbf{y}^{\mathrm{H}} \mathbf{\Gamma}_i^{-1} \mathbf{y} \right], \tag{31}$$

and $\mathbf{\Gamma}_i \in \mathbb{C}^{N_r \times N_r}$ is the co-variance matrix of $\mathbf{y}$ given by

$$\mathbf{\Gamma}_i = \frac{E_s}{N_u} \cdot \left[\sum_{k \in \mathcal{I}_i} \mathbf{h}_k \right] \left[\sum_{k \in \mathcal{I}_i} \mathbf{h}_k^{\mathrm{H}} \right] + N_0 \mathbf{I}. \tag{32}$$

Proof: Given the i-th spatial symbol, (27) describes a single stream being sent over an $N_u \times N_r$ MIMO channel. The mutual information is maximized when 1) s is ZMCG-distributed, i.e., $s \sim C\mathcal{N}(0, E_s)$, and 2) the received signal vector is maximal ratio combined [38, ch. 5]. Without CSIT, equal power is therefore allocated for different IQ channels, i.e, E_s is constant over i. It is straightforward to write the IQ domain capacity C_1 as

$$C_1 = \sum_i p(i) \left[\log_2 \left(1 + \frac{E_s}{N_0} \left\| \frac{1}{\sqrt{N_u}} \mathbf{H} \mathbf{e}_i \right\|^2 \right) \right], \tag{33}$$

which can be further written into the form in (30).

[4] By the singular value decomposition theorem, we have $\mathbf{H} = \mathbf{U}\mathbf{\Sigma}\mathbf{V}^{\mathrm{H}}$, where $\mathbf{U} \in \mathbb{C}^{N_r \times N_r}$ and $\mathbf{V} \in \mathbb{C}^{N_t \times N_t}$ are unitary, and $\mathbf{\Sigma} \in \mathbb{R}^{N_r \times N_t}$ is a diagonal rectangular matrix containing square roots of eigenvalues of $\mathbf{H}\mathbf{H}^{\mathrm{H}}$ (the same as those of $\mathbf{H}^{\mathrm{H}}\mathbf{H}$) listed in descending order from upper left to lower right. Due to (21), we have $\mathbf{H}^{\mathrm{H}}\mathbf{H} = \mathrm{diag}(N_r, \cdots, N_r) \in \mathbb{R}^{N_t \times N_t}$ and $\mathbf{\Sigma} = \mathrm{diag}(\sqrt{N_r}, \cdots, \sqrt{N_r})$ with N_t nonzero entries. The pseudo-inverse of $\mathbf{H}$ is given by $\mathbf{H}^{\dagger} = \mathbf{V}\mathbf{\Sigma}^{\dagger}\mathbf{U}^{\mathrm{H}}$, where $\mathbf{\Sigma}^{\dagger} = (\mathbf{\Sigma}^{\mathrm{H}}\mathbf{\Sigma})^{-1}\mathbf{\Sigma}^{\mathrm{H}}$. By multiplying $\mathbf{y}$ by $\sqrt{N_r}\mathbf{H}^{\dagger}$ we come up with (28).

Uniform distribution of i means $p(i) = 1/\binom{N_t}{N_u}$ and $H(i) = \log_2 \binom{N_t}{N_u}$. $H(i|\mathbf{y})$ can be calculated as

$$\begin{aligned} H(i|\mathbf{y}) &= \int_{\mathbf{y}} \sum_i p(\mathbf{y}, i) \log_2 \frac{1}{p(i|\mathbf{y})} \, \mathrm{d}\mathbf{y} \\ &= \frac{1}{\binom{N_t}{N_u}} \int_{\mathbf{y}} \sum_i p(\mathbf{y}|i) \log_2 \frac{\sum_{i'} p(\mathbf{y}|i')}{p(\mathbf{y}|i)} \, \mathrm{d}\mathbf{y} \\ &= \frac{1}{\binom{N_t}{N_u}} \sum_i \mathbb{E}_{\mathbf{y}|i} \left[\log_2 \frac{\sum_{i'} p(\mathbf{y}|i')}{p(\mathbf{y}|i)} \right]. \end{aligned} \tag{34}$$

Therefore, $C_2 = I(i;\mathbf{y}) = H(i) - H(i|\mathbf{y})$ is as given in (30). ∎

Theorem 2. *When the LOS MIMO channel is column orthogonal, the capacity achieved by LOS GSM-N_u with ZMCG signaling in the IQ domain and uniform signaling in the spatial domain is given by*

$$C = \underbrace{\log_2 \left(1 + N_r \frac{E_s}{N_0}\right)}_{C_1} + \underbrace{\log_2 \tbinom{N_t}{N_u} - \mathbb{E}_{\tilde{\mathbf{y}}|1} \left[\log_2 \tilde{\Psi}_i\right]}_{C_2}, \tag{35}$$

where

$$\tilde{\Psi}_i = 1 + \sum_{i'(i' \neq i)} \exp[-\tilde{\mathbf{y}}^{\mathrm{H}} (\tilde{\mathbf{\Gamma}}_{i'}^{-1} - \tilde{\mathbf{\Gamma}}_i^{-1}) \tilde{\mathbf{y}}], \tag{36}$$

the PDF of $\tilde{\mathbf{y}}$ given i is given by

$$p(\tilde{\mathbf{y}}|i) = \frac{1}{\left|\pi \tilde{\mathbf{\Gamma}}_i\right|} \exp\left[-\tilde{\mathbf{y}}^{\mathrm{H}} \tilde{\mathbf{\Gamma}}_i^{-1} \tilde{\mathbf{y}}\right] \quad , \tag{37}$$

and $\tilde{\mathbf{\Gamma}}_i \in \mathbb{R}^{\mathrm{N_t} \times \mathrm{N_t}}$ is the co-variance matrix of $\tilde{\mathbf{y}}$ given by

$$\tilde{\mathbf{\Gamma}}_i = \frac{N_r E_s}{N_u} \mathbf{e}_i \mathbf{e}_i^{\mathrm{T}} + N_0 \mathbf{I}. \tag{38}$$

Proof: Under condition (21), we have

$$\left\| \sum_{k \in \mathcal{I}_i} \mathbf{h}_k \right\|^2 = \sum_{k \in \mathcal{I}_i} \|\mathbf{h}_k\|^2 = N_r N_u, \tag{39}$$

and C_1 of (30) can be simplified into the form in (35). Under condition (21) and based on the equivalent channel model given in (28), it is trivial to write C_2 of (30) into the from in (35). Due to symmetry among $\{i\}$, i in $\mathbb{E}_{\tilde{\mathbf{y}}|i}[\cdot]$ can be arbitrarily chosen, therefore in (35) we write $\mathbb{E}_{\tilde{\mathbf{y}}|1}[\cdot]$. ∎

We have two remarks on (35): 1) We observe that the RX array introduces an array gain of N_r in C_1, but no array gain is achieved by the TX array; 2) In general, C_2 in (35) can not be further simplified. To evaluate it, we can resort to numerical methods e.g., Monte Carlo averaging.

The suboptimality of the above two step optimization of $I(i, s; \mathbf{y})$ lies in the fact that although Gaussian signaling of s maximizes $I(s;\mathbf{y}|i)$ and uniform signaling of i maximizes $H(i)$, it is not immediately clear if the sum of $I(s;\mathbf{y}|i)$ and $I(i;\mathbf{y})$ is maximized. Due to randomness, a Gaussian s is intuitively not an optimal signaling to maximize $I(i;\mathbf{y})$. As confirmed in Fig. 8(a), compared to the above C_2 which results from a Gaussian s, a constant s (over i) leads to a larger spatial mutual information which we denote as C_2'. The derivation of C_2' is similar to that of C_2 except for a constant s and therefore is omitted here. Note that due to a constant s, GSM simplifies into generalized space shift keying (GSSK) which transmits information only in the spatial domain. Therefore, $C_1 + C_2'$ is an upper bound that results from independent maximization of the two terms in $I(s;\mathbf{y}|i) + I(i;\mathbf{y})$. We will show in Fig. 8(a) that the upper bound is actually achieved by uniform i and ZMCG s at high SNR. At low SNR, the gap between $C_1 + C_2$ and $C_1 + C_2'$, however, is not significant.

C. Symbol Error Probability (SEP)

An upper bound SEP for GSM-N_u with ML detection, which is partly based on the union bound method [34], is given by

$$\begin{aligned} P_s \leq & \, \mathbb{E}_i \left[\Pr\left[\text{error in } m|i\right] \right] \\ & + \mathbb{E}_{i,m} \left[\sum_{i', m'(i' \neq i)} \Pr[(i,m) \to (i',m')|(i,m)] \right] \end{aligned} \tag{40}$$

where $\Pr\left[\text{error in } m|i\right]$ is the SEP in the IQ domain given the i-th spatial symbol, and $\Pr[(i,m) \to (i',m')|(i,m)]$ is the probability of (i',m') being detected given that (i,m) was sent. For conventional IQ constellations, the error probability is usually exactly known [35]. This not only makes (40) tighter than (6), but also makes evaluation of P_s more convenient.

Theorem 3. *When the LOS MIMO channel is column orthogonal, the SEP for LOS GSM-N_u is given by*

$$P_s \leq P_{\mathrm{iq}} + P_{\mathrm{sp}} + P_{\mathrm{joint}}, \tag{41}$$

where

$$P_{\mathrm{iq}} = P_m \left(N_r \frac{E_s}{N_0} \right) \tag{42}$$

with $P_m(\cdot)$ being the SEP of the IQ modulation, and

$$P_{\mathrm{sp}} = \frac{1}{M} \sum_m \sum_{đ=1}^{N_u} \tbinom{N_u}{N_u - đ} \tbinom{N_t - N_u}{đ} Q\left(\sqrt{\frac{đ N_r r_m^2}{N_u N_0}} \right) \tag{43}$$

$$\begin{aligned} P_{\mathrm{joint}} = & \frac{1}{M} \sum_m \sum_{\substack{m' \\ (m' \neq m)}} \sum_{đ=1}^{N_u} \tbinom{N_u}{N_u - đ} \tbinom{N_t - N_u}{đ} \times \\ & Q\left(\sqrt{\frac{(N_u - đ) N_r d_{mm'}^2 + đ N_r \left(r_m^2 + r_{m'}^2\right)}{2 N_u N_0}} \right). \end{aligned} \tag{44}$$

Proof: The proof is provided in Appendix B. ∎

In (41), P_{iq} is the average IQ SEP, P_{sp} is the average spatial SEP, and P_{joint} the average probability of the detection for the IQ and spatial symbols being simultaneously wrong.

V. Numerical Results and Further Analysis

The purpose of this section is twofold: 1) to develop a quantitative understanding of the performance achieved by LOS SM/GSM, including a look into the robustness of the scheme and the impact of not having perfect channel orthogonality, and 2) to compare the performance of SM/GSM with SMX and BF in (pure) LOS.

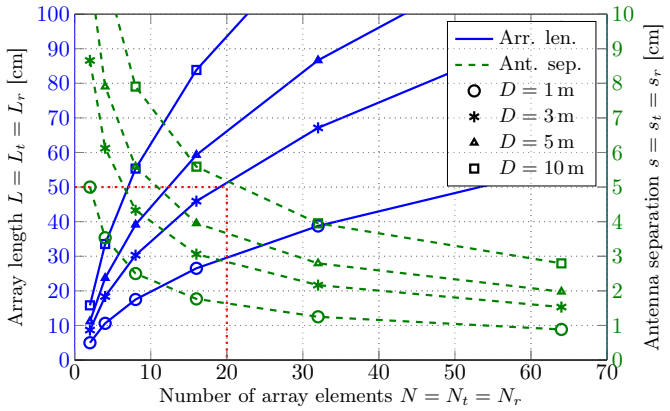

Fig. 5. Array length L and antenna separation s vs. the number of antennas N. Equal number of antennas, and equal antenna separations are assumed for TX and RX. The curves are generated according to (25) with $f = 60\,\mathrm{GHz}$ and $\zeta = 1$.

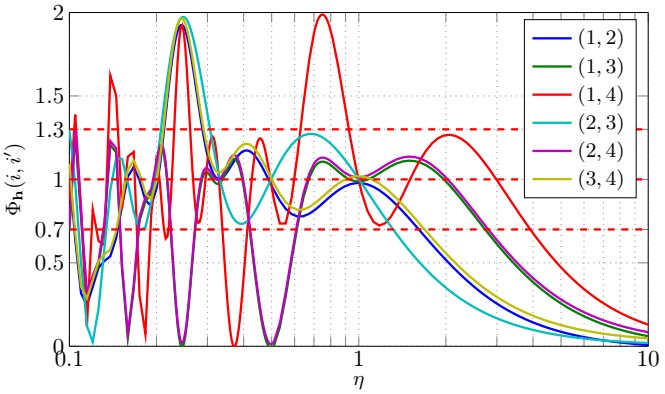

Fig. 6. Channel Euclidean distance $\Phi_{\mathbf{h}}(i,i')$ versus ASP deviation η. Artificial offsets within ± 0.02 are added to the curves to avoid overlaying.

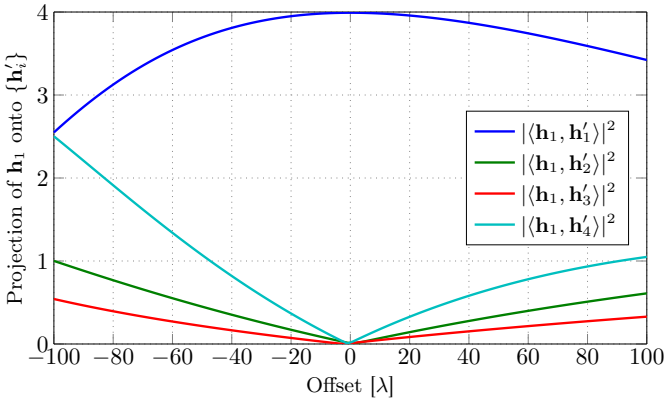

Fig. 7. Robustness of channel orthogonality against errors in CSIR due to a sudden change the relative geometric relations of the TX and RX arrays.

A. LOS MIMO Channel

1) Array Dimensions: To see the physical dimensions needed to achieve condition (21) at 60 GHz, in Fig. 5 we plot the array length L and antenna separation s versus the number of receive antennas N_r for various indoor-relevant TX-RX distances ($D = 1 - 10\,\mathrm{m}$) according to (25). We see that for typical indoor distances of a few meters and within an array length of $20 - 50\,\mathrm{cm}$, which lies within the dimensions of laptops, desktop PC monitors or HD TV's, setting up a perfectly orthogonal LOS MIMO channel with 10 to 20 (TX) antennas is possible.

2) Robustness: The optimal ASP to achieve channel orthogonality was found based on a deterministic analysis for given λ, D, and ζ. Perfect orthogonality can be achieved only at a single frequency for given D and ζ. Therefore, in this part, we investigate the robustness of the channel orthogonality against 1) a change of these parameters, and 2) errors in CSIR which may be caused by a sudden change of the relative geometric relations between the TX and RX arrays (because of user movement or vibration of the terminal).

At 60 GHz, a communication bandwidth of e.g., 2.16 GHz as used in IEEE802.11ad and Wireless HD [14], should be easily covered, since, if centered at 60 GHz, 2.16 GHz translates into a very small span of $\eta = 0.98 - 1.01$. Regarding the tilt factor ζ, since LOS MIMO relies on the broadside of the TX and RX arrays to face each other, ζ should not be too large. As an extreme example, if both arrays lie on the x-axis (see Fig. 2), we have $\zeta = \infty$ and the system cannot operate in an LOS mode. Below we assume parallel and aligned arrays, i.e., $\zeta = 1$ and investigate the impact of varying D.

We consider a 4×4 MIMO system with parallel and aligned ULAs, i.e., $\zeta = 1$ and $s_t = s_r = 5\,\mathrm{cm}$, where the $s_t s_r$ is chosen to be optimal, i.e., $\eta = 1$ for $D = 2\,\mathrm{m}$ at 60 GHz. The normalized channel Euclidean distance

$$\Phi_{\mathbf{h}}(i,i') = \frac{1}{2N_r} \|\mathbf{h}_i - \mathbf{h}_{i'}\|^2 \tag{45}$$

for various η are plotted in Fig. 6 by varying D from $0.2\,\mathrm{m}$ to $20\,\mathrm{m}$ (where $D = 0.2\,\mathrm{m}$ and $20\,\mathrm{m}$ respectively correspond to $\eta = 0.1$ and 10). We see that when η becomes large ($\eta \gg 1$) due to increased D, the channel Euclidean distances decrease and tend to vanish. When η becomes small ($\eta \ll 1$) due to decreased D, there are two kinds of variations of $\Phi_{\mathbf{h}}$ over η: 1) the full scale variations within the range $0 - 2$, and 2) the smaller variations within the range $0.7 - 1.3$. Comparing this with Fig. 10 in Section V-D, we find that the capacity in the high SNR regime is only sensitive to large variations of $\Phi_{\mathbf{h}}$, but not to the small variations. In Section V-D, we will provide a further in-dept analysis of the impact of the variations of $\Phi_{\mathbf{h}}$ on the GSM capacity.

To look into the impact of errors in CSIR due to a sudden change of the geometric relations between TX and RX arrays, we use the same 4×4 system as parameterized above, and obtain the perfect CSIR, i.e., $\{\mathbf{h}_i\}$ at $D = 2\,\mathrm{m}$. Then we move the RX by an offset within the range -100λ to 100λ and measure $\{\mathbf{h}'_i\}$. In Fig. 7, we project $\mathbf{h}_1$ on to $\{\mathbf{h}'_i\}$ and plot the energy. It is immediately clear that the orthogonality condition is not sensitive to CSIR errors due to an offset in the range of up to $\pm 20\lambda$ which, at 60 GHz, means $\pm 10\,\mathrm{cm}$.

B. Channel Capacity

In this subsection, we quantitatively study the capacity of GSM-MIMO in comparison with SMX-MIMO and BF-MIMO in LOS. The same number of TX and RX antennas are used in the comparison between GSM-MIMO and BF-MIMO since

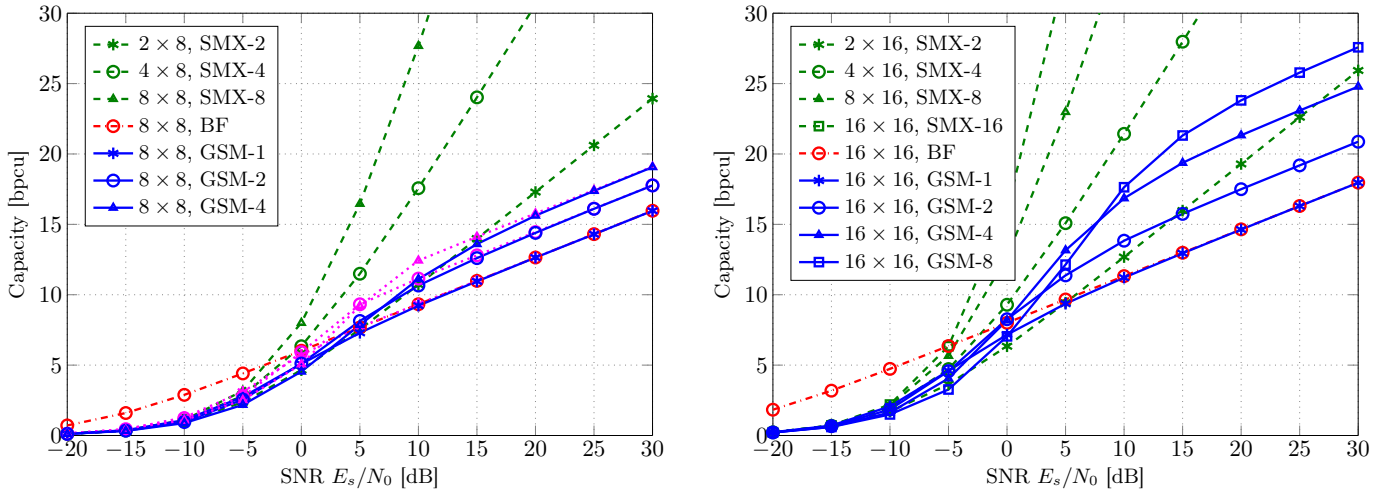

(a) (b)

Fig. 8. Capacity of GSM-MIMO in comparison with SMX-MIMO and BF-MIMO in orthogonal LOS channels. The magenta curves in (a) are upper bound capacities $C_1 + C_2'$ for the corresponding GSM-N_u schemes.

both schemes use a single TX chain. For SMX-MIMO, the number of RX antennas is the same as for the other schemes we consider, but we assume each TX antenna is equipped with a dedicated TX chain, i.e., in total N_t TX chains and the number of TX antennas is varied. The reason why different numbers of TX antennas are used in SMX-MIMO originates from the fact that the cost and power consumption are related to the number of RF chains [2], [14]. In GSM-MIMO we exploit larger number of antennas in a more energy-efficient manner by using a single TX chain.

The capacity of LOS GSM-N_u under the orthogonal channel condition (21) is plotted in Fig. 8 for different N_u's, and the capacities of LOS BF and LOS SMX [9], [11] are plotted for comparison. The array setup according to (25) is used for both GSM-N_u and SMX, and the curves for GSM-N_u and SMX are generated respectively according to (35) and the second (non-inline) equation on page 7 of [39]

$$C_{\mathrm{SMX}} = \log_2 \left| \mathbf{I}_{N_r} + \frac{P_t}{N_t N_0} \mathbf{H}\mathbf{H}^{\mathrm{H}} \right| = N_t \log_2 \left(1 + \frac{N_r P_t}{N_t N_0} \right), \tag{46}$$

where P_t is the total transmit power. For BF-MIMO in LOS, an upper bound for the capacity, which is achievable with spatial combining at the TX and maximal ratio combining (MRC) at the RX using antenna separations down to $\lambda/2$ [5], [6], is

$$C_{\mathrm{BF}} \leq \log_2 \left(1 + N_t N_r P_t / N_0 \right), \tag{47}$$

where P_t is the total transmit power. Therefore, the curves for BF are generated according to (47).

First we analyze the capacity of GSM-N_u. We see that GSM-1 achieves the same capacity as BF at moderate and high SNR. With more TX antennas activated per channel use, i.e., $N_u > 1$, GSM-N_u achieves higher capacity at moderate and high SNR. At low SNR, larger N_u leads to lower capacity, but the capacity differences between GSM-N_u with different N_u's are marginal. Since the upper limit of C_2 in (35) is $\log_2 \binom{N_t}{N_u}$ and $\binom{N_t}{N_u} = \binom{N_t}{N_t - N_u}$, at high SNR the largest capacity achieved by GSM-N_u is when $N_u = \lfloor N_t/2 \rfloor$. That is why the largest capacity achieved by GSM-N_u is shown in Fig. 8(a) by GSM-4 for 8×8 MIMO and in Fig. 8(b) by GSM-8 for 16×16 MIMO.

Comparison of GSM-N_u and SMX: As expected, SMX shows a huge capacity gain over GSM-N_u and BF. However, SMX needs N_t full TX chains to transmit N_t data streams. A major advantage of GSM lies in its simplicity due to the single-RF architecture. Actually as shown in Fig. 8(b), for large N_t and particularly when $N_u = \lfloor N_t/2 \rfloor$, a significant portion of the capacity gap between SMX and BF is filled up by GSM-N_u.

Comparison of GSM and BF: At high SNR, BF achieves the asymptotic capacity $\log_2(N_t N_r E_s/N_0)$. However, GSM-N_u has an asymptotic capacity of $\log_2(N_t N_r E_s/N_0) - \log_2(N_t) + \log_2 \binom{N_t}{N_u}$. Thus BF achieves the same capacity as GSM-1. Depending on N_u, the gap between the capacities of BF and GSM-N_u at high SNR can be large, despite the fact that GSM also only uses a single TX chain. The strength of BF is at low SNR, where it achieves a higher capacity than both GSM-N_u and SMX.

We remark that:

- At low SNR, BF gain is more important than SMX gain, i.e., BF is more suitable in the power-limited regime.
- GSM-N_u under the orthogonal channel condition does not achieve any TX array gain in the IQ domain, but it attains spatial domain capacity. The spatial domain capacity attained by GSM-1 at sufficient SNR is equal to the amount of capacity increase due the N_t-fold TX array gain in BF.
- It is thus shown that by separating the antennas appropriately and using GSM or SMX, much higher capacities than that of BF can be achieved in LOS.
- With GSM-N_u, we only need one TX RF chain, while SMX needs the same number of full TX chains (baseband and RF) as the number of data streams.

C. Symbol Error Probability (SEP)

In this subsection, we study the SEP of GSM-MIMO in comparison with SMX-MIMO and BF-MIMO in LOS. Similarly as in Section V-B, the same number of TX and RX antennas are used in the comparison between GSM-MIMO and BF-MIMO. For SMX-MIMO, the number of RX antennas is the same as for the other schemes we consider, but we assume each TX antenna is equipped with a dedicated TX chain and the number of TX antennas is varied. Different from Section V-B is that here the purpose is to compare the error probabilities for the same data rate. Therefore the parameters N_t, N_u and M are chosen, on top of the aforementioned assumptions, in a way that the same data rate is achieved with different schemes.

The SEP for GSM-N_u versus per-bit-SNR E_b/N_0 is plotted in Fig. 9 for data rates of $6\,\mathrm{bpcu}$, $8\,\mathrm{bpcu}$ and $16\,\mathrm{bpcu}$ respectively in three subfigures[5]. The curves for GSM-N_u, BF and SMX are generated respectively according to (41), (57) and (59), and these SEP expressions are validated by simulated results that are indicated in Fig. 9(a) by magenta dots. Furthermore, the simulated results show that the upper bound given by (41) becomes tight at moderate and high SNR.

It is shown in (41) that the SEP of GSM-N_u depends on the IQ symbol distances $\{d_{mm'}\}$ and magnitudes $\{r_m\}$, and the distance between the spatial symbols $\{\mathrm{đ}_{ii'}\}$. Optimized error performance is expected if we make a balanced use of the parameters N_t, N_u and M. We notice in Fig. 9 that to achieve the given rates, GSM-N_u with 4-QAM outperforms both GSM-N_u with 1-QAM[6] and GSM-N_u with $M(M>4)$-QAM. Therefore, to achieve a certain data rate, keeping $M=4$ and moving to larger N_u is more efficient than keeping a small N_u and moving to a larger M than 4.

Comparison of GSM-N_u and SMX: As expected, for a fixed data rate SMX with larger number of TX antennas and lower order QAM in general performs better than a configuration with smaller number of streams but with higher order QAM. In Fig. 9(b), 8×8 MIMO using GSM-4 with 4-QAM performs similar as 4×8 MIMO using SMX with 4-QAM, despite the fact that the latter has much higher capacity as shown in Fig. 8(a). In Fig. 9(c), 16×16 MIMO using GSM-8 with 4-QAM performs only marginally worse than 8×16 MIMO using SMX with 4-QAM, despite the fact that the latter has much higher capacity as shown in Fig. 8(b).

Comparison of GSM-N_u and BF: In Fig. 9(a), BF can achieve relatively good error performance at a data rate of $6\,\mathrm{bpcu}$. However, to achieve higher data rates BF requires higher order QAM, which always gives (much) worse error performance compared to GSM-N_u. This again shows that BF is a suitable scheme only in the power-limited regime for lower data rates.

D. Impact of Non-Orthogonal Channel on GSM Capacity

In this subsection, we investigate the impact of not having perfect channel orthogonality, i.e. $\eta \neq 1$. In order to take advantage of Fig. 6, we use exactly the same set of parameters of the 4×4 system that was used to generate Fig. 6, and similarly we vary D from $0.2\,\mathrm{m}$ to $20\,\mathrm{m}$. The capacities of GSM-1 and GSM-2 are simulated according to (30) at "high SNR" $E_s/N_0 = 15\,\mathrm{dB}$ and plotted in Fig. 10 with respect to η.

First we consider GSM-1 and analyze C_1 and C_2 separately. If we ignore any approximation errors due to (2), in (30) $\|\mathbf{H}\mathbf{e}_i/\sqrt{N_u}\|^2 = N_r$ is a constant and C_1 does not depend on η. The first part of C_2 in (30), i.e. $H(i)$, is constant. However, the second part, $H(i|\mathbf{y})$, which measures the average uncertainty of i given $\mathbf{y}$, depends on the Euclidean distance between the spatial symbols. The larger the Euclidean distance between the spatial symbols, the less is the uncertainty of i given $\mathbf{y}$ at a certain SNR level, and vice versa. It is shown in Fig. 6 that when $\eta<1$, which means the actual ASP is larger than the optimal value, the Euclidean distance between some channel pairs can become 0, thus making detection of those pairs impossible. For example, because of $\Phi_{\mathbf{h}}(1,3)=0$ and $\Phi_{\mathbf{h}}(2,4)=0$ in Fig. 6 at $\eta=0.5$, which implies that there are only two distinguishable spatial symbols, C_2 in Fig. 10 at $\eta=0.5$ reduces to $1\,\mathrm{bpcu}$. When η increases above 1, which means the actual ASP is smaller than the optimal value, as expected the spatial capacity decreases. However, even at $\eta=10$, i.e, $D=20\,\mathrm{m}$, more than $1\,\mathrm{bpcu}$ of the spatial capacity is still attained.

Now we consider GSM-2. Unless the channel is perfectly orthogonal, $\{\mathbf{h}_k\}_{k\in\mathcal{I}_i}$ in (30) can add both constructively and destructively thus causing C_1 to vary. When η gets larger than 1, the vectors $\{\mathbf{h}_k\}_{k\in\mathcal{I}_i}$ move closer to each other and tend to add constructively. This means that when $\eta>1$, GSM-N_u ($N_u>1$) can exploit some TX array gain and larger η suggests higher C_1. Apparently the upper limit of C_1 is equal to the capacity of an $N_u\times N_r$ BF-MIMO. When η gets larger than 1, C_2 of GSM-2 drops faster than in the case of GSM-1. As shown in Fig. 10, at $\eta=10$, C_2 of GSM-2 ends up with the same value as GSM-1. This means that when the spatial degree of freedom is limited due to insufficient ASP, creating more spatial symbols by switching on a larger number of TX antennas per symbol does not lead to a higher spatial domain capacity.

On one hand, good capacity is achieved under the orthogonal channel condition at $\eta=1$, and, overall, the total capacity C of GSM-N_u is rather robust over η. On the other hand, the maximum total capacity for GSM-2 is reached at $\eta=4$ but not $\eta=1$, thus showing the sub-optimality of the orthogonal channel condition (see also Fig. 4).

When the normalized channel Euclidean distance $\Phi_{\mathbf{h}}(i,i')$ is too small, i.e., close to 0, it becomes difficult or impossible to distinguish the pair of $\mathbf{h}_i$ and $\mathbf{h}_{i'}$, thus implying a reduction of the spatial domain performance; when $\Phi_{\mathbf{h}}(i,i')$ is too large,

[5]For the GSM-N_u curves, the actual data rate can be slightly different from the nominal rate R, e.g., in the case of 16×16 MIMO using GSM-4 and 64-QAM the exact rate is $16.83\,\mathrm{bps}$, instead of $R=16\,\mathrm{bpcu}$.

[6]GSM-N_u with 1-QAM is actually GSSK with N_u TX antennas activated per channel use (a.k.a. GSSK-N_u).

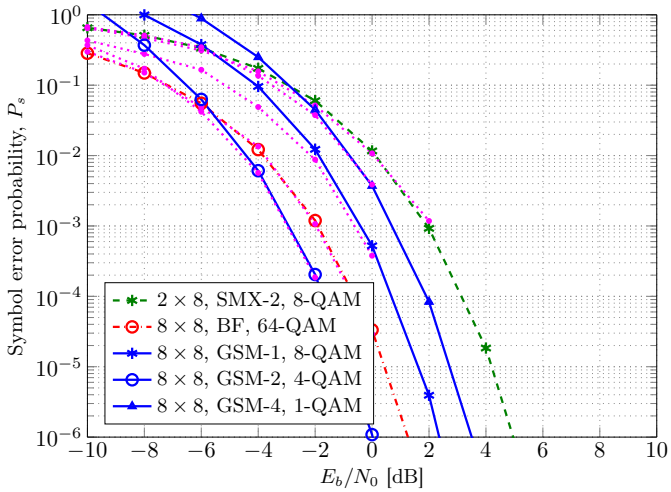

(a) $R = 6$ bpcu

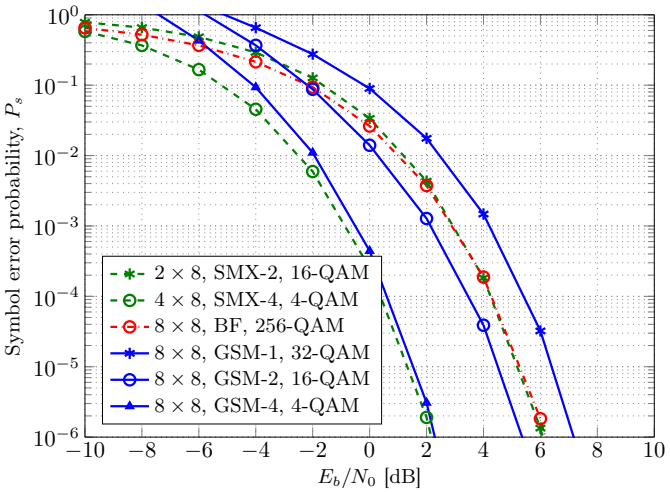

(b) $R = 8$ bpcu

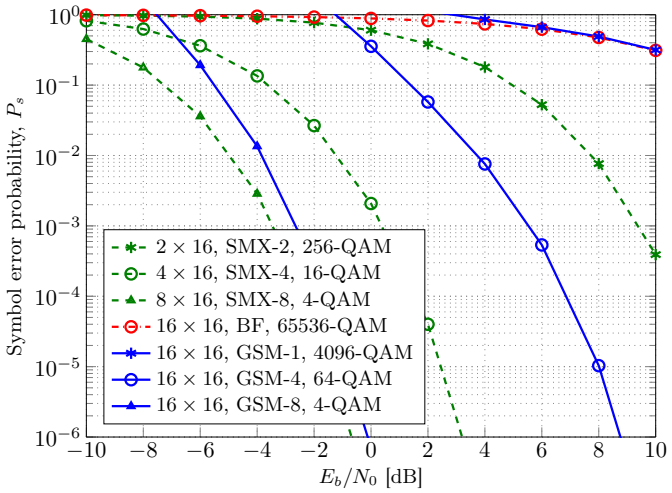

(c) $R = 16$ bpcu

Fig. 9. SEP of GSM-N_u versus SMX and BF for $N_t \times N_r$ MIMO in orthogonal LOS channels. The magenta curves in (a) are simulated results.

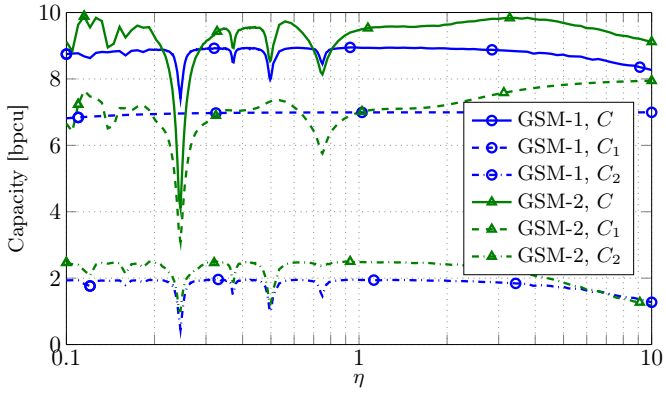

Fig. 10. Capacity of GSM-N_u versus ASP deviation factor η. Simulated according to (30) with $N_t = N_r = 4$ and $E_s/N_0 = 15$ dB.

i.e., close to 2, the pair of $\mathbf{h}_i$ and $\mathbf{h}_{i'}$ cancel each other, thus implying a reduction of the IQ domain performance. Therefore, the channel Euclidean distance as a partial channel information may be needed for the TX to adapt for optimized operation by skipping or grouping together some of the TX antennas.

VI. Practical Implementation

Although SM/GSM has been extensively researched at low-GHz frequencies and has shown to be a simple scheme in concept, its practical implementation has not been sufficiently addressed [18] and remains an open issue. In this section, we try to address this issue by proposing two novel hardware architectures — one for TX and one for RX — with special considerations for implementation at mmWave frequencies. The proposed TX and RX are shown in Fig. 11, and, in what follows, we introduce their working principles and show some simulation results.

A. TX

The implementation of fixed-N_u GSM at mmWave frequencies is facing the following main challenges: 1) fast N_u-to-N_t switching at symbol rate, 2) large routing loss due to the excess

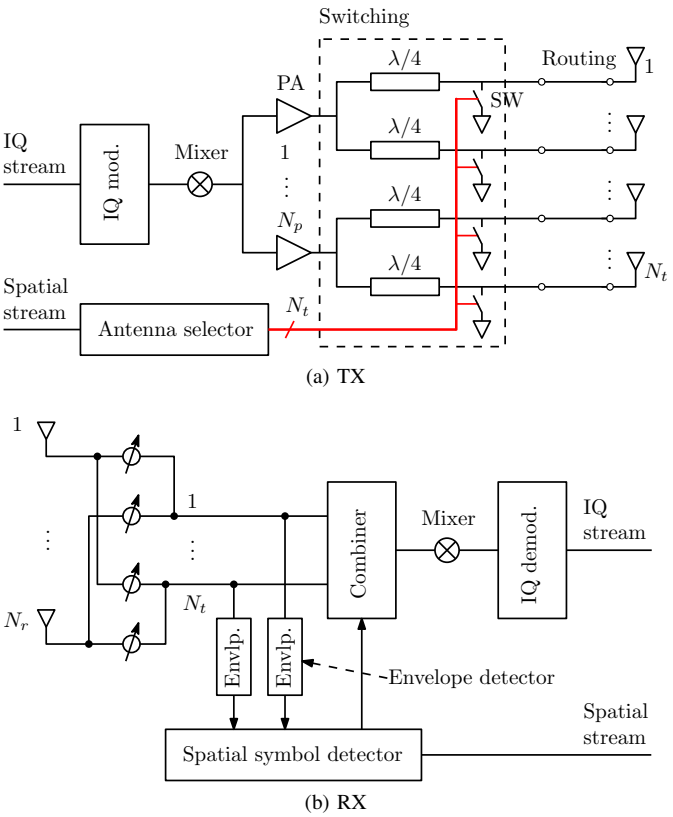

Fig. 11. Proposed TX and RX for LOS SM/GSM at mmWave frequencies.

antenna separations necessary to achieve optimized SEP in LOS, and 3) tight link power budget due to limited output power of mmWave PAs, lossy routing and high FSPL at mmWave frequencies. We therefore propose a novel TX architecture that is shown in Fig. 11(a) to address these issues.

In the proposed TX, the (single) modulated IQ signal is up-converted to RF and split into N_p branches, each of which is equipped with a PA. And each PA is connected to a sub-group of TX antennas, out of which a fixed number which is smaller than N_u is activated, but the total number of activated antennas must be N_u. For example, in a system with $N_t = 8$, $N_u = 4$ and $N_p = 2$, we can let each sub-group contain $N_t/N_p = 4$ antennas and activate $N_u/N_p = 2$ antennas from each sub-group within each time slot. The switching within each sub-group of TX antennas is based on the single-pole multi-throw (SPMT) switching structure of [40], but in our case more than one TX antennas may have to be activated within each time slot. A TX antenna is activate and deactivated respectively by switching OFF and ON the corresponding shunt switch (SW). The quarter-wave transformer serves two purposes: 1) when an SW is ON, it transforms the short circuit into an open circuit; 2) to match the total load impedance of the activated (or non-short-circuited) branches to the source impedance. The switching speed should not be a bottleneck, since the shunt SWs are just single-pole double-throw (SPDT) switches, which have been reported to be able to switch at a maximum rate of 13 GHz (rise/fall time: 25/50 ps) [41].

The selection of N_p is mainly a consideration of the total transmit power and the routing loss. Increasing N_p can increase the total transmit power and reduce the routing loss (because each PA would then only need to cover a smaller number of adjacent TX antennas). In this paper, we stick to $N_p = 1$, which leads to the simplest implementation with single-RF.

B. RX

At the RX, we have to detect the IQ symbol and the indices of the activated TX antennas in order to recover the IQ and spatial streams, either jointly or separately [12], [33], [42]. Depending on the detection strategy, the architecture and complexity of the RX may look differently. For example, an ML detector [33] may require N_r full RX chains and this may be acceptable only for small scale (i.e., small N_r) systems. For large scale systems, the cost and power consumption of mmWave components [14], [15] force us to consider other cost-effective and power-efficient RX architectures. Therefore we propose the RX architecture in Fig. 11(b), which features hybrid RF/digital processing and separate detection of the IQ and spatial streams.

In the proposed RX, we use RF phase shifters to equalize the received signal vector, which is largely motivated by the hybrid architecture for mmWave SMX MIMO [15]. The purpose of the $N_t \times N_r$ equalizer matrix, which is formed by the phase shifters, is to separate the $N_r \times N_t$ MIMO channel into N_t individual SISO channels, which correspond to the N_t branches as shown in Fig. 11(b). In each time slot, the spatial symbol is detected by identifying the N_u branches that contain an IQ symbol. Since the equalization is conducted at RF, the detection of the presence of an IQ symbol at each branch is just a matter of detecting the magnitude of the signal. For this purpose, we can use the envelope detectors that are widely used in non-coherent on-off keying (OOK) receivers [43], [44]. The spatial symbol detector may use N_t low-resolution or even 1-bit ADCs. Based on the detected spatial symbol, the N_u detected branches are combined (e.g., using MRC), down-converted to baseband, and quantized in full resolution for IQ symbol detection. As a result, we need N_t low-resolution ADCs for spatial symbol detection, and one mixer and two full resolution ADCs for IQ symbol detection. The hardware complexity has been greatly reduced thus making the scheme practical for large N_t and N_r. This is in contrast to the ML RX, which needs N_r mixers and $2N_r$ full resolution ADCs.

C. Simulated SEP

For an exemplary demonstration of the SEP performance using the proposed TX and RX, we assume a 8×8 system with parallel and aligned ULAs (i.e., $\zeta = 1$), and choose an ASP such that the channel is orthogonal at $D = 3\,\mathrm{m}$. The component values and link parameters are listed in Table I. Furthermore, we use a zero forcing (ZF) equalizer, i.e., $\mathbf{H}^{\mathrm{H}}$, for simulation. More precisely, we apply only the phases of $\mathbf{H}^{\mathrm{H}}$ to the corresponding phase shifters. The spatial symbol detection is based on a strategy of finding the N_u (out of N_t) maxima of the magnitudes of the equalized signals. For IQ detection, the detected N_u equalized signals are simply summed up and an ML detector is applied to detect the IQ symbol. Since the RX scheme used in the simulation features

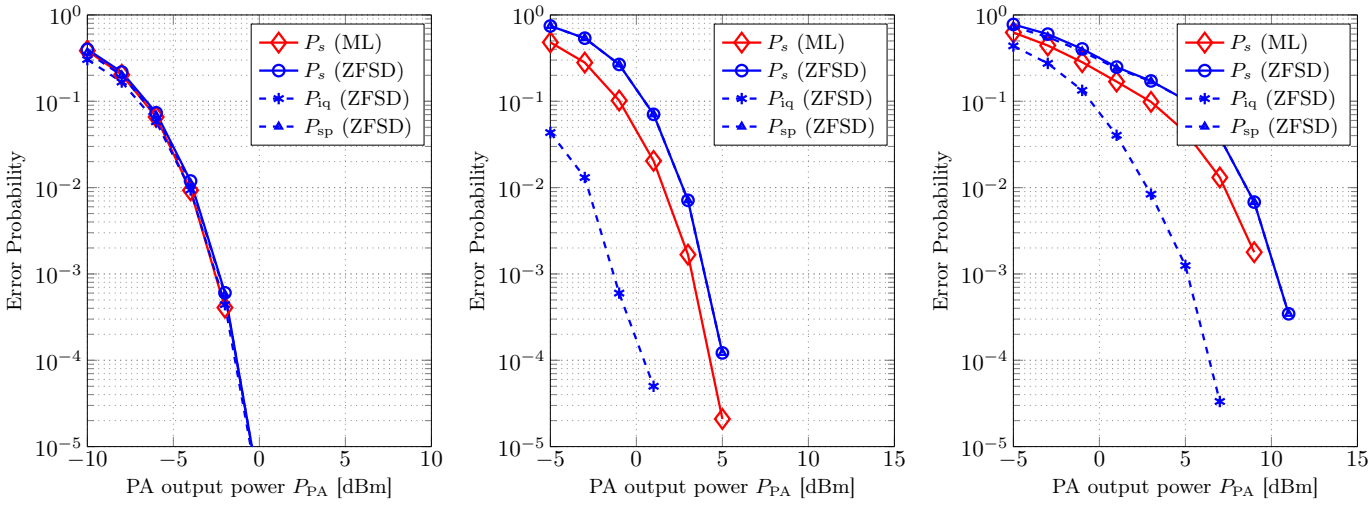

(a) GSM-1 with 4-QAM (b) GSM-4 with 4-QAM (c) GSM-4 with 16-QAM

Fig. 12. Simulated error probability of a 8×8 LOS GSM system using the proposed TX and RX. Detailed simulation parameters are listed in Table I.

TABLE I
LINK BUDGET FOR LOS SM/GSM USING THE PROPOSED TX†

Center frequency	GHz	60
Bandwidth	GHz	1
PA output power [45, TABLE 1]	dBm	P_{PA} ($P_{-1\,\mathrm{dB}} \leq 19.7$)
Switch insertion loss [40], [46]	dBm	3
Routing loss (0.04 dB/mm [47])	dBm	6
TX antenna gain	dBi	5
FSPL over 3 m	dB	77.6
RX antenna gain	dBi	9
Noise power (290 K)	dBm	-84
RX noise figure [48], [49]	dB	6
SNR (TX power to noise power)	dB	$P_{\mathrm{PA}} + 5.4$

† The system is 8×8 and with parallel and aligned ULAs, i.e., $\zeta = 1$. A single PA is assumed, i.e., $N_p = 1$. The TX and RX antenna separations are $s_t = s_r = 4.3\,\mathrm{cm}$, which achieve perfect channel orthogonality at $D = 3\,\mathrm{m}$. Moderate TX and RX antenna gains are assumed.

both ZF equalization and separation detection, we denote it as ZFSD. The simulation results are plotted in Fig. 12. We see that in the case of GSM-1 with 4-QAM in Fig. 12(a), ZFSD achieves the ML performance. In the case of GSM-4 with 4-QAM and 16-QAM respectively in Fig. 12(b) and Fig. 12(c), the error performance of ZFSD is within 1 dB to ML[7]. These results confirm that our proposed RX has a very promising error performance.

VII. CONCLUSION

In this paper, we studied LOS SM/GSM for indoor mmWave communication at 60 GHz. We sought to optimize the error performance of SM in LOS by maximizing the minimum Euclidean distance of received SM symbols. As a result, we found that the error performance of LOS SM/GSM can be optimized by making the channel matrix column-orthogonal. We derived the capacity and SEP for LOS SM/GSM and presented numerical results which gave insight into the behavior and performance of SM/GSM in LOS. Finally, we proposed novel TX and RX hardware architectures for implementation of SM/GSM at mmWave frequencies. Overall, we have shown that LOS SM/GSM is a promising scheme, especially for short-range indoor mmWave communications, in which the short wavelength enables us to pack a large number of antennas within the device dimensions. On-going research is concerned with an exact analysis of the power efficiency of the proposed TX architecture and an in-depth analysis of the proposed RX architecture.

[7]Since, for GSM-4, P_{iq} is considerably lower than P_{sp}, and P_s is determined by P_{sp}, the less than 1 dB penalty is mainly due to the error performance deterioration in the spatial domain.

APPENDIX A
DERIVATION OF $\Phi_{\min}$ FOR THE CASE $i \neq i'$ AND $m \neq m'$

In the case of $i \neq i'$ and $m \neq m'$, Φ in (8) can be written into

$$\Phi = N_r \left[r_m^2 + r_{m'}^2 - 2 r_m r_{m'} \Re \left\{ e^{\mathrm{j}\vartheta(m,m')} \cos\theta_{\mathrm{C}}(i,i') \right\} \right] \tag{48}$$

where $\vartheta(m,m') = \angle q_{m'} - \angle q_m$ is the angle between the 2-D vectors q_m and $q_{m'}$, and $\theta_{\mathrm{C}}(i,i')$ a complex-valued angle between $\mathbf{h}_i$ and $\mathbf{h}_{i'}$ as given by [36]

$$\cos\theta_{\mathrm{C}}(i,i') = \frac{\langle \mathbf{h}_i, \mathbf{h}_{i'} \rangle}{\|\mathbf{h}_i\| \|\mathbf{h}_{i'}\|}. \tag{49}$$

According to [36, (3)–(5)], we can express $\cos\theta_{\mathrm{C}}(i,i')$ as

$$\cos\theta_{\mathrm{C}}(i,i') = \cos\theta_{\mathrm{H}}(i,i') e^{\mathrm{j}\varphi(i,i')}, \tag{50}$$

where $\cos\theta_{\mathrm{H}}(i,i') = |\cos\theta_{\mathrm{C}}(i,i')|$ is the ratio between the length of the orthogonal projection (with respect to the Hermitian product) of vector $\mathbf{h}_i$ onto vector $\mathbf{h}_{i'}$ to the length of $\mathbf{h}_i$ [36], $\theta_{\mathrm{H}}(i,i') \in [0, \pi/2]$ is called the Hermitian angle, and

$\varphi(i,i') \in [-\pi,\pi]$ is called the Kasner's pseudo angle. Now we can write (48) into

$$\begin{aligned}\Phi &= N_r \Big[r_m^2 + r_{m'}^2 - 2 r_m r_{m'} \\ &\quad \times \Re\left\{ \cos\theta_{\mathrm{H}}(i,i') e^{\mathbb{j}\left[\varphi(i,i')+\vartheta(m,m')\right]} \right\} \Big] \\ &= N_r \Big[r_m^2 + r_{m'}^2 - 2 r_m r_{m'} \\ &\quad \times \cos\theta_{\mathrm{H}}(i,i') \cos\left[\varphi(i,i')+\vartheta(m,m')\right] \Big].\end{aligned} \tag{51}$$

Since $\cos\left[\varphi(i,i')+\vartheta(m,m')\right] \le 1$, a lower bound for $\Phi_{\min}$ is therefore found to be (14a).

Appendix B
Proof of Theorem 3

The $\Pr[(i,m)\to(i',m')|(i,m)]$ in (40) can be written into

$$\begin{aligned}&\Pr[(i,m)\to(i',m')|(i,m)] \\ &= \Pr\left[\left\| \mathbf{y} - \frac{q_{m'}}{\sqrt{N_u}}\mathbf{H}\mathbf{e}_{i'} \right\|^2 < \left\| \mathbf{y} - \frac{q_m}{\sqrt{N_u}}\mathbf{H}\mathbf{e}_i \right\|^2 \right] \\ &= \Pr\Bigg[\left\| \frac{q_m}{\sqrt{N_u}}\mathbf{H}\mathbf{e}_i - \frac{q_{m'}}{\sqrt{N_u}}\mathbf{H}\mathbf{e}_{i'} \right\|^2 \\ &\qquad < \underbrace{2\Re\left\{ \left(\frac{q_{m'}}{\sqrt{N_u}}\mathbf{H}\mathbf{e}_{i'} - \frac{q_m}{\sqrt{N_u}}\mathbf{H}\mathbf{e}_i \right)^{\mathrm{H}} \mathbf{n} \right\}}_{n_\Sigma} \Bigg] \\ &= Q\left(\sqrt{\frac{\Phi}{2N_0}} \right),\end{aligned} \tag{52}$$

where n_Σ, which is a simplified notation for $n_\Sigma(i,m,i',m')$, is Gaussian distributed

$$n_\Sigma \sim \mathcal{N}\left(0, 2\left\| \frac{q_{m'}}{\sqrt{N_u}}\mathbf{H}\mathbf{e}_{i'} - \frac{q_m}{\sqrt{N_u}}\mathbf{H}\mathbf{e}_i \right\|^2 N_0 \right),$$

Φ, which is a simplified notation for $\Phi(i,m,i',m')$, is the squared Euclidean distance between two GSM symbols

$$\Phi = \left\| \frac{q_m}{\sqrt{N_u}}\mathbf{H}\mathbf{e}_i - \frac{q_{m'}}{\sqrt{N_u}}\mathbf{H}\mathbf{e}_{i'} \right\|^2. \tag{53}$$

Under condition (21), Φ in (53) can be written into

$$\Phi_{m\neq m'} = \frac{|q_m - q_{m'}|^2}{N_u} \cdot \left\| \sum_{k\in\mathcal{I}_i} \mathbf{h}_k \right\|^2 = N_r d_{mm'}^2, \tag{54}$$

$$\begin{aligned}\Phi_{i\neq i'} &= \frac{r_m^2}{N_u} \cdot \left\| \sum_{k\in\mathcal{I}_i} \mathbf{h}_k - \sum_{k'\in\mathcal{I}_{i'}} \mathbf{h}_{k'} \right\|^2 \\ &= \frac{r_m^2}{N_u} \cdot \left[\left\| \sum_{k\in\mathcal{I}_i\setminus\mathcal{I}_{i'}} \mathbf{h}_k \right\|^2 + \left\| \sum_{k'\in\mathcal{I}_{i'}\setminus\mathcal{I}_i} \mathbf{h}_{k'} \right\|^2 \right] \\ &= \frac{2\mathrm{đ}_{ii'} N_r r_m^2}{N_u}\end{aligned} \tag{55}$$

where $d_{mm'} = |q_m - q_{m'}|$ is the IQ symbol distance, $\mathrm{đ}_{ii'} = \left|\mathcal{I}_i \setminus \mathcal{I}_{i'}\right| = \left|\mathcal{I}_{i'} \setminus \mathcal{I}_i\right|$ is the number of antennas activated by e_i but not by $e_{i'}$, or by $e_{i'}$ but not by e_i, and

$$\begin{aligned}\Phi_{\substack{i\neq i' \\ m\neq m'}} &= \frac{1}{N_u} \cdot \left\| q_m \sum_{k\in\mathcal{I}_i} \mathbf{h}_k - q_{m'} \sum_{k'\in\mathcal{I}_{i'}} \mathbf{h}_{k'} \right\|^2 \\ &= \frac{1}{N_u} \Bigg[\left\| (q_m - q_{m'}) \sum_{k\in\mathcal{I}_i\cap\mathcal{I}_{i'}} \mathbf{h}_k \right\|^2 \\ &\quad + \left\| q_m \sum_{k\in\mathcal{I}_i\setminus\mathcal{I}_{i'}} \mathbf{h}_k \right\|^2 + \left\| q_{m'} \sum_{k'\in\mathcal{I}_{i'}\setminus\mathcal{I}_i} \mathbf{h}_{k'} \right\|^2 \Bigg] \\ &= \frac{1}{N_u} \left[\left(N_u - \mathrm{đ}_{ii'}\right) N_r d_{mm'}^2 + \mathrm{đ}_{ii'} N_r \left(r_m^2 + r_{m'}^2 \right) \right].\end{aligned} \tag{56}$$

By the definition of $\mathrm{đ}_{ii'}$, there is $\mathrm{đ}_{ii'} = \|\mathbf{e}_i - \mathbf{e}_{i'}\|^2/2$, where $\|\mathbf{e}_i - \mathbf{e}_{i'}\|^2$ is the hamming distance between $\mathbf{e}_i$ and $\mathbf{e}_{i'}$. By considering (54) and plugging (39), (55), (56) and (52) into (40), we come up with (41).

Appendix C
SEP of BF-MIMO and SMX-MIMO in LOS

In BF-MIMO, ideally N_t-fold TX array gain and N_r-fold RX array gain can be simultaneously achieved by using spatial combining at TX and MRC at RX [6] [5], therefore the best achievable SEP for BF-MIMO using rectangular M-QAM is [35], [50]

$$P_{s,\mathrm{BF}} = P_{\mathrm{m}}\left(N_t N_r E_s/N_0\right) = 1 - P(M_I,d)P(M_Q,d) \tag{57}$$

where $d = \sqrt{12 N_t N_r E_s/(M_I^2 + M_Q^2 - 2)}$, M_I and M_Q are respectively the number of signal levels in the in-phase and quadrature dimensions, i.e., $M = M_I M_Q$, and

$$P(M,d) = 1 - 2\left(1 - 1/M\right) Q\left(d \Big/ \sqrt{2N_0} \right). \tag{58}$$

The SEP for SMX-MIMO, which simultaneously sends N_t rectangular M-QAM streams, is found by considering the equivalent channel model [39, Section 3.1] and using independent detection of the N_t streams [35], [50] as

$$P_{s,\mathrm{SMX}} = 1 - \left[P(M_I,d)P(M_Q,d)\right]^{N_t} \tag{59}$$

where $d = \sqrt{12 N_r E_s/N_t/(M_I^2 + M_Q^2 - 2)}$, and M_I and M_Q are respectively the number of signal levels in the in-phase and quadrature dimensions, i.e., $M = M_I M_Q$, and $P(M,d)$ is as given in (58).

References

[1] S. K. Yong and C.-C. Chong, "An overview of multigigabit wireless through millimeter wave technology: Potentials and technical challenges," *EURASIP J. Wirel. Commun. Netw.*, vol. 2007, no. 1, pp. 50–50, Jan. 2007.

[2] Z. Pi and F. Khan, "An introduction to millimeter-wave mobile broadband systems," *IEEE Commun. Mag.*, vol. 49, no. 6, pp. 101–107, Jun. 2011.

[3] T. S. Rappaport *et al.*, "Millimeter wave mobile communications for 5g cellular: It will work!" *IEEE Access*, vol. 1, pp. 335–349, 2013.

[4] R. Daniels *et al.*, "60 GHz wireless: Up close and personal," *IEEE Microw. Mag.*, vol. 11, no. 7, pp. 44–50, Dec. 2010.

[5] A. Valdes-Garcia *et al.*, "A fully integrated 16-element phased-array transmitter in SiGe BiCMOS for 60-GHz communications," *IEEE J. Solid-State Circuits*, vol. 45, no. 12, pp. 2757–2773, Dec. 2010.

[6] A. Natarajan *et al.*, "A fully-integrated 16-element phased-array receiver in SiGe BiCMOS for 60-GHz Communications," *IEEE J. Solid-State Circuits*, vol. 46, no. 5, pp. 1059–1075, May 2011.

[7] A. Ulusoy *et al.*, "A 60 GHz multi-Gb/s system demonstrator utilizing analog synchronization and 1-bit data conversion," in *2013 IEEE 13th Topical Meeting on Silicon Monolithic Integrated Circuits in RF Systems (SiRF)*, Jan. 2013, pp. 99–101.

[8] W. Roh *et al.*, "Millimeter-wave beamforming as an enabling technology for 5g cellular communications: theoretical feasibility and prototype results," *IEEE Commun. Mag.*, vol. 52, no. 2, pp. 106–113, Feb. 2014.

[9] F. Bohagen *et al.*, "Construction and capacity analysis of high-rank line-of-sight MIMO channels," in *2005 IEEE Wireless Communications and Networking Conf.*, vol. 1. IEEE, 2005, pp. 432–437.

[10] T. Ingason and H. Liu, "Line-of-sight MIMO for microwave links — Adaptive dual polarized and spatially separated systems," Master Thesis, Chalmers University Of Technology, Göteborg, Sweden, Jul. 2009.

[11] E. Torkildson *et al.*, "Indoor millimeter wave MIMO: Feasibility and performance," *IEEE Trans. Wireless Commun.*, vol. 10, no. 12, pp. 4150–4160, Dec. 2011.

[12] R. Mesleh *et al.*, "Spatial modulation — A new low complexity spectral efficiency enhancing technique," in *1st Int. Conf. on Communications and Networking in China*, Oct. 2006, pp. 1–5.

[13] A. Stavridis *et al.*, "Energy evaluation of spatial modulation at a multi-antenna base station," in *2013 IEEE 78th Vehicular Technology Conf. (VTC Fall)*, Sep. 2013, pp. 1–5.

[14] R. W. Heath, "Millimeter wave MIMO: A signal processing perspective," Apr. 2015. [Online]. Available: http://users.ece.utexas.edu/~rheath/presentations/2015/MmWaveMIMOaSPPerspectiveICASSP2015Heath.pdf

[15] O. E. Ayach *et al.*, "Spatially sparse precoding in millimeter wave MIMO systems," *IEEE Trans. Wireless Commun.*, vol. 13, no. 3, pp. 1499–1513, Mar. 2014.

[16] A. Younis *et al.*, "Generalised spatial modulation," in *2010 Conf. Rec. of the 44th Asilomar Conf. on Signals, Systems and Computers (ASILOMAR)*. IEEE, 2010, pp. 1498–1502.

[17] ——, "Performance analysis for generalised spatial modulation," in *Proc. 20th European Wireless Conf.*, May 2014, pp. 1–6.

[18] M. Di Renzo *et al.*, "Spatial modulation for generalized MIMO: Challenges, opportunities, and implementation," *Proc. IEEE*, vol. 102, no. 1, pp. 56–103, Jan. 2014.

[19] D. Gesbert *et al.*, "MIMO wireless channels: capacity and performance prediction," in *IEEE Global Telecommunications Conf., 2000. GLOBECOM '00*, vol. 2, 2000, pp. 1083–1088 vol.2.

[20] ——, "Outdoor MIMO wireless channels: models and performance prediction," *IEEE Trans. Commun.*, vol. 50, no. 12, pp. 1926–1934, Dec. 2002.

[21] N. Serafimovski *et al.*, "Practical Implementation of Spatial Modulation," *IEEE Trans. Veh. Technol.*, vol. 62, no. 9, pp. 4511–4523, Nov. 2013.

[22] A. Younis *et al.*, "Performance of Spatial Modulation Using Measured Real-World Channels," in *2013 IEEE 78th Vehicular Technology Conf. (VTC Fall)*, Sep. 2013, pp. 1–5.

[23] J. Zhang *et al.*, "Bit Error Probability of Spatial Modulation over Measured Indoor Channels," *IEEE Trans. Wireless Commun.*, vol. 13, no. 3, pp. 1380–1387, Mar. 2014.

[24] A. Maltsev *et al.*, "Channel models for 60 GHz WLAN systems," Tech. Rep. IEEE 802.11-09/0334r8, May 2010. [Online]. Available: https://mentor.ieee.org/802.11/dcn/09/11-09-0334-08-00ad-channel-models-for-60-ghz-wlan-systems.doc

[25] N. Valliappan *et al.*, "Antenna subset modulation for secure millimeter-wave wireless communication," *IEEE Trans. Commun.*, vol. 61, no. 8, pp. 3231–3245, Aug. 2013.

[26] P. Liu and A. Springer, "Space shift keying for LOS communication at mmWave frequencies," *IEEE Wireless Commun. Lett.*, vol. 4, no. 2, pp. 121–124, Apr. 2015.

[27] N. Serafimovski *et al.*, "Fractional bit encoded spatial modulation (FBE-SM)," *IEEE Commun. Lett.*, vol. 14, no. 5, pp. 429–431, May 2010.

[28] Y. Yang and S. Aissa, "Bit-padding information guided channel hopping," *IEEE Commun. Lett.*, vol. 15, no. 2, pp. 163–165, Feb. 2011.

[29] H. Friis, "A note on a simple transmission formula," *Proceedings of the IRE*, vol. 34, no. 5, pp. 254–256, May 1946.

[30] A. Maltsev *et al.*, "Statistical channel model for 60 GHz WLAN systems in conference room environment," *Radioengineering*, vol. 20, no. 2, pp. 409–422, Jun. 2011.

[31] M. R. Akdeniz *et al.*, "Millimeter wave channel modeling and cellular capacity evaluation," *arXiv:1312.4921 [cs]*, Dec. 2013, arXiv: 1312.4921. [Online]. Available: http://arxiv.org/abs/1312.4921

[32] L. L. Yang, "60ghz: Opportunity for gigabit WPAN and WLAN convergence," *SIGCOMM Comput. Commun. Rev.*, vol. 39, no. 1, pp. 56–61, Dec. 2008.

[33] J. Jeganathan *et al.*, "Spatial modulation: optimal detection and performance analysis," *IEEE Commun. Lett.*, vol. 12, no. 8, pp. 545–547, Aug. 2008.

[34] M. Di Renzo and H. Haas, "Performance analysis of spatial modulation," in *2010 5th Int. ICST Conf. on Communications and Networking in China (CHINACOM)*. IEEE, 2010, pp. 1–7.

[35] J. Proakis and M. Salehi, *Digital Communications, 5th Edition*, 5th ed. Boston: McGraw-Hill Science/Engineering/Math, Nov. 2007.

[36] K. Scharnhorst, "Angles in Complex Vector Spaces," *Acta Applicandae Mathematicae*, vol. 69, no. 1, pp. 95–103, 2001, arXiv: math/9904077. [Online]. Available: http://arxiv.org/abs/math/9904077

[37] Y. Yang and B. Jiao, "Information-guided channel-hopping for high data rate wireless communication," *IEEE Commun. Lett.*, vol. 12, no. 4, pp. 225–227, Apr. 2008.

[38] D. Tse and P. Viswanath, *Fundamentals of Wireless Communication*. Cambridge, UK ; New York: Cambridge University Press, Jul. 2005.

[39] E. Telatar, "Capacity of multi-antenna gaussian channels," *Eur. Trans. on Telecommun.*, vol. 10, no. 6, pp. 585–595, Nov. 1999.

[40] Y. A. Atesal *et al.*, "Low-loss 0.13-μm CMOS 50–70 GHz SPDT and SP4T switches," in *2009 IEEE Radio Freq. Integr. Circuits Symp.*, vol. 1. IEEE, jun 2009, pp. 43–46.

[41] I. Kallfass *et al.*, "Multiple-throw millimeter-wave FET switches for frequencies from 60 up to 120 GHz," in *2008 European Microwave Integrated Circuit Conf.*, Oct. 2008, pp. 426–429.

[42] J. Wang *et al.*, "Generalised spatial modulation system with multiple active transmit antennas and low complexity detection scheme," *IEEE Trans. Wireless Commun.*, vol. 11, no. 4, pp. 1605–1615, Apr. 2012.

[43] F. Lin *et al.*, "A low power 60GHz OOK transceiver system in 90nm CMOS with innovative on-chip AMC antenna," in *IEEE Asian Solid-State Circuits Conf., 2009*, Nov. 2009, pp. 349–352.

[44] J. J. Lee and C. S. Park, "60-GHz gigabits-per-second OOK modulator with high output power in 90-nm CMOS," *IEEE Trans. Circuits Syst. II*, vol. 58, no. 5, pp. 249–253, May 2011.

[45] Y. Zhao and J. R. Long, "A wideband, dual-path, millimeter-wave power amplifier with 20 dBm output power and PAE above 15% in 130 nm SiGe-BiCMOS," *IEEE Journal of Solid-State Circuits*, vol. 47, no. 9, pp. 1981–1997, 2012.

[46] R. L. Schmid *et al.*, "A compact, transformer-based 60 GHz SPDT RF switch utilizing diode-connected SiGe HBTs," in *2013 IEEE Bipolar/BiCMOS Circuits and Technology Meeting (BCTM)*. IEEE, sep 2013, pp. 111–114.

[47] "Taconic TacLamplus datasheet." [Online]. Available: http://www.taconic-add.com/pdf/taclamplus.pdf

[48] Y. Yu *et al.*, *Integrated 60GHz RF Beamforming in CMOS*. Dordrecht: Springer Netherlands, 2011.

[49] H.-C. Kuo and H.-R. Chuang, "A 60-GHz high-gain, low-power, 3.7-dB noise-figure low-noise amplifier in 90-nm CMOS," in *2013 European Microwave Integrated Circuits Conf.*, Oct. 2013, pp. 584–587.

[50] N. Beaulieu, "A useful integral for wireless communication theory and its application to rectangular signaling constellation error rates," *IEEE Trans. Commun.*, vol. 54, no. 5, pp. 802–805, May 2006.